Universität Bremen

ALFRED-WEGENER-INSTITUT
HELMHOLTZ-ZENTRUM FÜR POLAR- UND MEERESFORSCHUNG

Improving the Description of the Formation of $CaCO_3$ in a Global Biogeochemical Model

Author

Md Razib Vhuiyan

Reviewers

Prof. Dr. Gerrit Lohmann

Dr. Christoph Völker

MASTERS THESIS

SUBMITTED IN PARTIAL FULFILMENT OF THE REQUIREMENTS FOR THE DEGREE OF

MASTER OF SCIENCE IN ENVIRONMENTAL PHYSICS

Supervised by

Dr. Christoph Völker

Institute of Environmental Physics and Remote Sensing (IUP-IFE)

University of Bremen, Bremen, Germany

December 23rd, 2016

pep

Declaration

I, Md. Razib Vhuiyan, herewith declare that I did the written work on my own and only with the means as indicated.

_____	_____
Date	Signature

Abstract

The formation of $CaCO_3$ in the ocean is an important process affecting the exchange of CO_2 with the atmosphere, especially on longer timescales. Formation of $CaCO_3$ in the largest part of the open ocean is mostly done by planktonic organisms, coccolithophores, foraminifera and to lesser degree pteropods. $CaCO_3$ that is formed near the ocean surface mostly sinks through the water column, often together with organic debris and dissolves at depth where the solubility product of $CaCO_3$ in its two main crystal forms (calcite and aragonite) increases due to the increase in pressure. Formation and dissolution of $CaCO_3$ affect both dissolved inorganic carbon and total alkalinity and hence CO_2. For this reason, biogeochemical ecosystem models often include the cycling of $CaCO_3$. Here the production of $CaCO_3$ is analyzed in the global biogeochemical model REcoM. In REcoM, biogenic $CaCO_3$ production is limited to phytoplankton only and is strictly proportional to the growth of the small phytoplankton model compartment. It is assumed that, a constant fraction of the small phytoplankton consists of coccolithophores and that these have a constant ratio between $CaCO_3$ and organic carbon. When the model is integrated over a thousand years under a monthly climatological forcing, REcoM output shows that with these assumptions, the alkalinity begins to deviate strongly with respect to the available observations. For the standard set of parameters of the ecosystem model, a transfer of alkalinity is identified from the ocean surface to the deep ocean, mostly in the depth range between 1700 m to 2000 m. Changes in the freshwater or salinity distribution but more likely an unrealistic distribution of $CaCO_3$ production and dissolution in the model are possible explanations. In this study, it is tested that whether changes in the parameterization of the $CaCO_3$:POC ratio in the model can improve the alkalinity distribution. A simple reduction in the ratio leads to a much improved alkalinity distribution but with an export of $CaCO_3$ of 0.343 Pg C yr^{-1} which is slightly lower than the estimation of [Berelson et al., 2007]. Furthermore, a more complicated dependency of the $CaCO_3$: POC production rate on temperature, nutrients and biomass suggested by [Aumont and Bopp, 2006] does not lead to a significant improvement on alkalinity distribution. Formation of $CaCO_3$ in the form of aragonite and dependency of the dissolution of $CaCO_3$ on seawater saturation state are neglected in REcoM.

Acknowledgment

I would like to thank my thesis supervisor Dr. Christoph Völker for his superb guidance and especially for the step by step planning throughout the thesis. I would also like to thank Dr. Völker for all his programming tips and for helping me to learn the usage of various programming languages and tools. I would like to thank Prof. Dr. Gerrit Lohmann for his guidance for developing the thesis structure. I would like to thank Prof. Dr. Dieter Wolf-Gladrow for allowing me in his research group. I would like to thank Prof. Dr. Jelle Bijma for answering my questions regarding phytoplankton. I would also like to thank the Alfred Wegener Institute and the IUP at the University of Bremen for welcoming me into their institute. Thank you to all of the people who contributed to the MITgcm and REcoM models. I would like to thank Essowe Panassa and Anna Pagnone for their friendly motivation throughout the thesis period. Thanks to Flora for her lovely motivation and sacrifices throughout the Masters Programme. Most of all, I would like to thank my parents and family members for all of their support and sacrifices.

Contents

List of Figures

Abbreviations

CCD	Calcite Compensation Depth
CORE	Common Ocean-Ice Reference Experiment
CR	Calcification Ratio
DIC	Dissolved Inorganic Carbon
DOC	Dissolved Organic Carbon
DON	Dissolved Organic Nitrogen
GLODAP	Global Ocean Data Analysis Project
GPP	Gross Primary Production
MITgcm	Massachusetts Institute of Technology general circulation model
NPP	Net Primary Production
PIC	Particulate Inorganic Carbon
PISCES	Pelagic Interactions Scheme for Carbon and Ecosystem Studies
POC	Particulate Organic Carbon
REcoM	Regulated Ecosystem Model
TA	Total Alkalinity
WOA09	World Ocean Atlas 2009

1 Introduction

1.1 Production and export of $CaCO_3$ in the ocean

Calcium carbonate is one of the most common minerals on earth's surface. Several crystal forms of $CaCO_3$ exist, of which the two most abundant are calcite and aragonite. In the ocean, calcite can represent a significant fraction of shelf and deep sea sediments. The mineral $CaCO_3$ is formed in the open ocean by biological processes and the precipitation of $CaCO_3$ is mainly done by three different types of phytoplankton and heterotrophic zooplankton [Sarmiento and Gruber, 2006, chapter 9, p.362]. Coccolithophorids which are a group of photosynthetic unicellular algae form an outer sphere made out of small calcite plates. In coccolithophorids, the $CaCO_3$ platelets (liths) are formed in special coccolith vesicles. After the formation of liths, they are transported to the outside portion of the cell and stay within a coccosphere until they are shed individually after the death of the cell or sometimes earlier [Sarmiento and Gruber, 2006, chapter 9]. Foraminifera which are unicellular amoeba-like organisms generally form a shell made out of calcite and pteropods which are free-swimming snails produce a shell made out of aragonite instead of calcite [Sarmiento and Gruber, 2006, chapter 9, p.362]. Evolutionary history is likely the key determinant for which mineral phase organisms precipitate because surface waters are supersaturated with respect to both mineral phases [Sarmiento and Gruber, 2006, chapter 9,]. Some marine organisms such as foraminifera precipitate $CaCO_3$ shells for protection against enemies, for others the reason for calcification is still debated. The formation of $CaCO_3$ from Ca^{2+} and HCO_3^- produces aqueous CO_2 and is hypothesized to be used as a source of inorganic carbon during photosynthesis of coccolithophorids [Paasche, 1962, Sikes et al., 1980, Sarmiento and Gruber, 2006]. [Zondervan, 2001] showed a very clear dependence of calcification rates by coccolithophorids on the availability of aqueous CO_2, with calcification rates plummeting as the aqueous CO_2 concentration increases. An excessive amount of CO_2 produced by human activity is taken up by the ocean through atmosphere-ocean gas exchange and results in more acidified oceans. Calcification in the ocean thus may be reduced in the future, due to the decreasing ocean pH caused by the rise of CO_2 in the atmosphere [Gattuso and Hansson, 2011].

The global carbonate production within the open ocean, i.e. vertically integrated calcification rate in the surface (euphotic layer) is estimated to be between 0.5 and 1.6 Gt of particulate

inorganic carbon (PIC) yr^{-1}, whereas the export, i.e. the vertical flux out of the productive upper layer of the ocean, the so-called euphotic zone, is between 0.4 and 1.8 Gt PIC yr^{-1} [Berelson et al., 2007]. The estimation is done by analyzing the $CaCO_3$ rain ratio (the ratio between the export of organic carbon and $CaCO_3$) into sediment traps and dissolution on sea floor. On the other hand the range of recent global estimates of organic matter production is 40-50 Gt of particulate organic matter (POC) yr^{-1} whereas the export ranges between 10 and 15 Gt C yr^{-1} [Jin et al., 2007]. [Henson et al., 2012] estimated that the amount of POC export is about 5 Gt C yr^{-1} but this is still debated. Her export estimation of POC was done by analyzing global patterns in particle export efficiency, the proportion of primary production that is exported from the surface ocean and transfer efficiency, the fraction of exported organic matter that reaches the deep ocean. The removal or export of dissolved inorganic carbon occur from the upper ocean either as $CaCO_3$ or as particulate organic carbon (POC). The ratio between rate of $CaCO_3$ export and rate of POC export defines the rain rate ratio [p.77 Zeebe and Wolf-Gladrow, 2001, chapter 1]. The estimated range of the global rain ratio is between $1/4$ to $1/14$. Changes in rain ratio possibly have contributed to glacial – interglacial CO_2 change (the 'rain- ratio hypothesis') [Archer et al., 2000].

1.2 Dissolution of $CaCO_3$ in the ocean

$CaCO_3$ particles that are produced biologically in the upper layers of ocean are potentially subject to dissolution which is primarily driven by the state of saturation of water with respect to the produced mineral phase (calcite and aragonite) [chapter 9, Sarmiento and Gruber, 2006, p. 365] . The dissolution reaction equilibrium relationship of a specific $CaCO_3$ mineral defines the solubility product ($K_{sp}^{\mathrm{CaCO_3}}$),

$$K_{sp}^{\mathrm{CaCO_3}} = [\mathrm{CO_3^{2-}}]_{sat} \times [\mathrm{Ca^{2+}}]_{sat} \tag{1}$$

[chapter 9, Sarmiento and Gruber, 2006, p.365] which has different value for calcite and aragonite. The degree of saturation (Ω) is defined as the ratio of the product of the solutes over the product of the solutes at saturation (solubility product) [chapter 9, Sarmiento and Gruber, 2006, p. 365]. For both $CaCO_3$ mineral phases, the degree of saturation (Ω) is:

$$\Omega = \frac{[\mathrm{CO_3^{2-}}] \times [\mathrm{Ca^{2+}}]}{[\mathrm{CO_3^{2-}}]_{sat} \times [\mathrm{Ca^{2+}}]_{sat}} = \frac{[\mathrm{CO_3^{2-}}] \times [\mathrm{Ca^{2+}}]}{K_{sp}^{\mathrm{CaCO_3}}} \tag{2}$$

[chapter 9, Sarmiento and Gruber, 2006, p.365] where the solubility product for aragonite and calcite needs to be taken respectively. Ω values larger than one are an indication of over-saturation and Ω values smaller than one an indication of under-saturation [Battaglia et al., 2016]. With respect to both $CaCO_3$ mineral phases, the upper ocean waters are generally supersaturated and deep ocean waters are under-saturated. Relatively little dissolution therefore occurs in the upper ocean and substantial dissolution starts when $CaCO_3$ particle enter the under-saturated zones of the water column. The solubility products of both calcite and aragonite depend strongly on pressure and relatively weakly on temperature [Berelson et al., 2007]. The observed difference in the solubilities and CO_3^{2-} saturation concentrations between surface water and deep ocean waters is about a factor of 3 [chapter 9, Sarmiento and Gruber, 2006, p. 368]. Generally aragonite has an average 50 percent higher solubility than calcite. Saturation horizons are defined as the depth horizon that separates supersaturated waters from under-saturated waters. The depth of the saturation horizons differs from ocean to ocean depending upon the mineral solubility and variations in ambient CO_3^{2-} concentration.

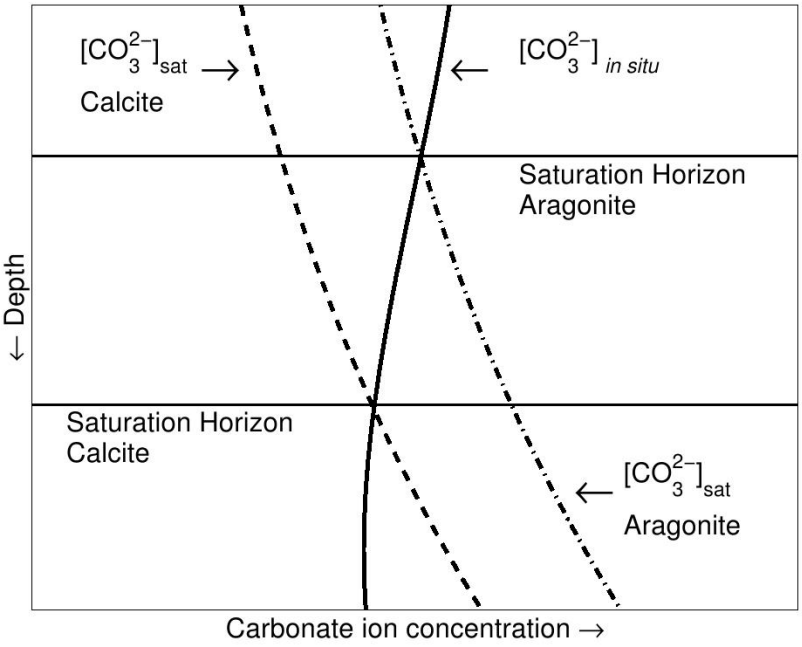

Figure 1: *A schematic illustration of the saturation horizons of calcite and aragonite in the ocean and how they are related to the increase in the saturation concentration CO_3^{2-} with depth. [p.25 Zeebe and Wolf-Gladrow, 2001, chapter 1]*

Dissolved Inorganic Carbon (DIC) increases in the deep ocean due to remineralisation of POC (Particulate Organic Carbon); this causes older water in the deep Pacific to have a higher DIC than in the relatively freshly ventilated deep Atlantic; increasing DIC decreases CO_3^{2-}, as long as alkalinity does not change too much, so the deep water in the Pacific has lower CO_3^{2-} and is more corrosive for $CaCO_3$ [Battaglia et al., 2016]. The saturation horizon with respect to calcite is therefore deepest in the North Atlantic (more than 4500 m) and shallowest in the North Pacific (less than 1000 m). For aragonite it lies at about 3000 m to 3500 m depth in the Atlantic while for the Pacific, it is within the main thermocline and almost reaches the surface in the North Pacific [Sarmiento and Gruber, 2006, chapter 9, p.368].

The $CaCO_3$ particles produced near the surface start to dissolve once they start sinking through the water column towards under-saturated water layers. An estimate of the dissolution kinetics of $CaCO_3$ when the water is under-saturated ($\Omega < 1$) can be done by:

$$\frac{d[\mathrm{CaCO_3}]}{dt} = -[\mathrm{CaCO_3}] \times k_{\mathrm{CaCO_3}}(1-\Omega)^n, \quad \text{for} \quad \Omega < 1 \tag{3}$$

[chapter 9, Sarmiento and Gruber, 2006, p.377]. This equation is a first order reaction, where $[CaCO_3]$ is the concentration of $CaCO_3$ (Unit: mmol/m^3), k_{CaCO_3} is the dissolution rate constant (Unit: day^{-1}) and the exponent n (which is often assumed to be $n = 1$) represents an apparent "order" of the reaction [Arvidson et al., 2003]. Carbonate mineral particles often sink and settle fast with a sinking velocity of more than 100 m day^{-1} because of their high density [Berelson et al., 2007]. A fraction of $CaCO_3$ dissolves already in the upper 1000 m of ocean, even in supersaturated waters with respect to calcite [Sarmiento and Gruber, 2006, chapter 9, p.371]. One possible explanation is that during travel from water surface to depth, dissolution occurs by corrosion driven by the saturation state of seawater, in connection with biological transformation and microbial oxidation of organic matter in sinking material which creates an acidic micro-environment conducive to dissolution [Alldredge and Cohen, 1987].

A little dissolution occurs already within the water column but most of the dissolution takes place within the sediments. In the sediment, the dissolution of $CaCO_3$ can also decouple from the depth of the saturation horizon. Some dissolution occurs already at the upper limit of the transition zone (so-called lysocline). Deeper, at the Calcite Compensation Depth (CCD) the sediments have lost all the calcite due to dissolution [Sarmiento and Gruber, 2006, chapter 9, p.374]. Below the CCD, the dissolution of $CaCO_3^{2-}$ in the sediment matches exactly the deposition at the top of the sediment [Broecker and Takahashi, 1977]. The depth of the lysocline

is broadly consistent with the depth of the saturation horizon. This consistency suggests that the thermodynamic driving factor is the dominant factor determining $CaCO_3$ preservation [p.376 Sarmiento and Gruber, 2006, chapter 9].

The ratio of particulate organic carbon to $CaCO_3$ that is deposited on the top of sediments is on average of the order of 1:1 or higher [Emerson and Bender, 1981, Archer, 1991]. This means that enough CO_2 is produced through organic matter remineralisation to potentially dissolve all $CaCO_3$ in the sediments, even above the saturation horizon.

1.3 Effects of formation and dissolution of $CaCO_3$ on the global carbon cycle

Formation and dissolution of $CaCO_3$ affect the carbonate system in the ocean by changing dissolved inorganic carbon (DIC) and total alkalinity (TA). DIC represents the total concentration of non-ionized CO_2, HCO_3^- and CO_3^{2-} of the ocean water [Zeebe and Wolf-Gladrow, 2001, chapter 1, p.27]. TA is the sum of carbonate alkalinity ($[HCO_3^-] + 2[CO_3^{2-}]$), borate alkalinity ($[B(OH)_4^-]$) and water alkalinity ($[OH^-]$ - $[H^+]$), plus a small contribution from other ions (nitrate, phosphate and silicate) [Zeebe and Wolf-Gladrow, 2001, chapter 1, p.29]. Both, the pH and the concentrations of carbonate species in the ocean are governed by the distribution of DIC and TA [Zeebe and Wolf-Gladrow, 2001, chapter 1, p.8]. The surface distribution of DIC and alkalinity determine the partial pressure of CO_2 in sea water and by that the CO_2 exchange with the atmosphere [Sarmiento and Gruber, 2006, chapter 9]

As shown in figure (2), invasion of CO_2 into the ocean (e.g. from anthropogenic sources) increases DIC and release of CO_2 to the atmosphere decreases DIC. But TA remains unchanged in both cases. This happens because in both processes the charge balance is not affected [Zeebe and Wolf-Gladrow, 2001, chapter 1, p.7]. $CaCO_3$ formation in contrast decreases both DIC and TA in the ocean in a ratio of 1:2 [Zeebe and Wolf-Gladrow, 2001, chapter 1, p.7]. This happens because, the precipitation of one mole $CaCO_3$ reduces DIC by one mole and either reduces CO_3^{2-} by one mole, or HCO_3^- by two moles [Zeebe and Wolf-Gladrow, 2001, chapter 1, p.76]. As a result, the system shifts to higher CO_2 levels and lower pH. A reduction in DIC and a slight increase in TA is caused by photosynthesis [Zeebe and Wolf-Gladrow, 2001, chapter 1, p.51]. The reason is that in addition to inorganic carbon, nutrients are taken up. The DIC variations

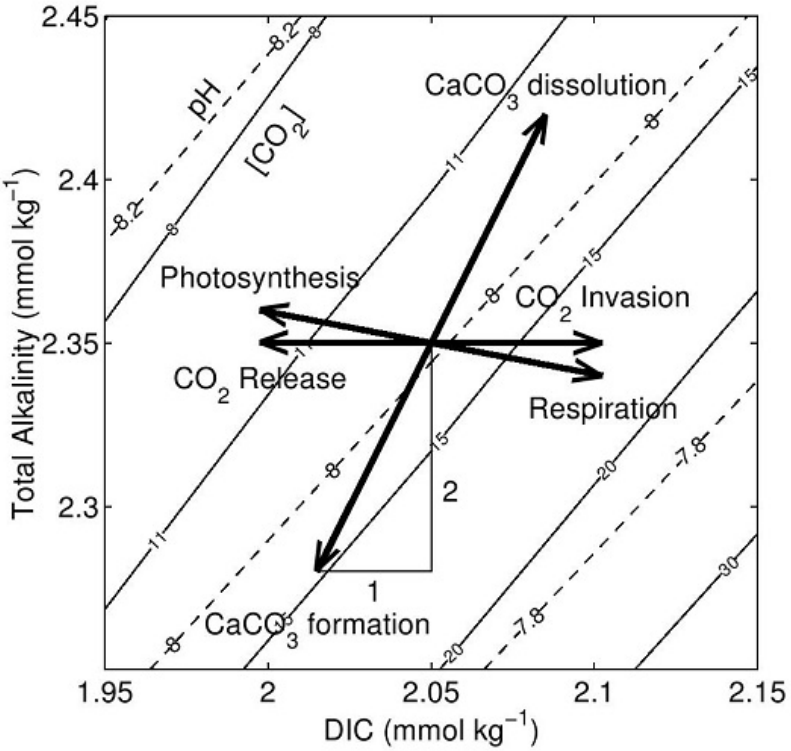

Figure 2: *Effect of various biogeochemical processes on DIC and TA and the resulting change in equilibrium pH (dashed lines) and [CO_2] (solid lines). [Zeebe and Wolf-Gladrow, 2001, chapter 1, p.7]*

caused by formation and dissolution of $CaCO_3$ in the ocean amount to maximally about 100 μmol kg^{-1}[chapter 9, Sarmiento and Gruber, 2006, p.366]. An increase in DIC results in a decrease in $CO_3{}^{2-}$ and a decrease in DIC results in an increase in $CO_3{}^{2-}$ as long as alkalinity remains more or less unchanged in both cases. But an increase in amount of $CaCO_3$ will lead to a decrease in alkalinity and a decrease in $CaCO_3$ to an increase in alkalinity. The difference between alkalinity and DIC is to first order equal to the $CO_3{}^{2-}$ concentration in the ocean.

2 Model

2.1 Description of the model

The model that is used in this study for understanding $CaCO_3$ formation and dissolution and its consequences for the carbon cycle on a global scale is a combination of the Massachusetts Institute of Technology general circulation model (MITgcm) [Marshall et al., 1997] and version 2 of the Regulated Ecosystem Model (REcoM). In this combination, MITgcm calculates the physical state of the ocean, including the circulation and mixing of tracers. MITgcm is a numerical model which is developed for the study of the ocean, atmosphere and climate for both small and large scale processes due to its non-hydrostatic capabilities [Marshall et al., 1997]. It is known to operate efficiency on multi processor systems over a large range of processor numbers and computer architectures [Losch et al., 2008]. The MITgcm ocean model is based on the Boussinesq approximation and it conserves volume rather than mass [Stammer et al., 2003]. Velocities, temperature and salinity are used as prognostic variables and tracers in the ocean in this model [Adcroft et al., 2004].

REcoM is a relatively simple ecosystem model which describes the biogeochemistry in the ocean including inorganic and organic forms of the main nutrients, two phytoplankton functional types (diatoms and nanophytoplankton), one zooplankton and one detritus compartment [Hauck et al., 2013]. REcoM adds several new biogeochemical tracers (e.g. concentrations of DIC, TA, dissolved nutrients and the biomasses) and calculates the biological or geochemical rates of change of the tracers. REcoM is based on the model by [Geider et al., 1998] that allows phytoplankton to adapt their stoichiometry to light and temperature conditions and to nutrient supply. The ratios of C:N and C:Chl are therefore variable in response to different growth conditions [Hauck et al., 2013]. $CaCO_3$ production is assumed to be a function of the gross nanophytoplankton production.

As shown in figure (3), the model carries two phytoplankton groups containing carbon, nitrogen, chlorophyll and either calcium carbonate or silicate. Phytoplankton can either be grazed by zooplankton or transformed into detritus through aggregation. Zooplankton biomass consists of carbon and nitrogen pools. Aggregation, mortality and faecal pellets of the zooplankton also produce detritus. Detritus, which contains organic carbon, nitrogen, biogenic silica and $CaCO_3$ sinks. In the course of the sinking, the particulate organic matter is degraded by bacteria to

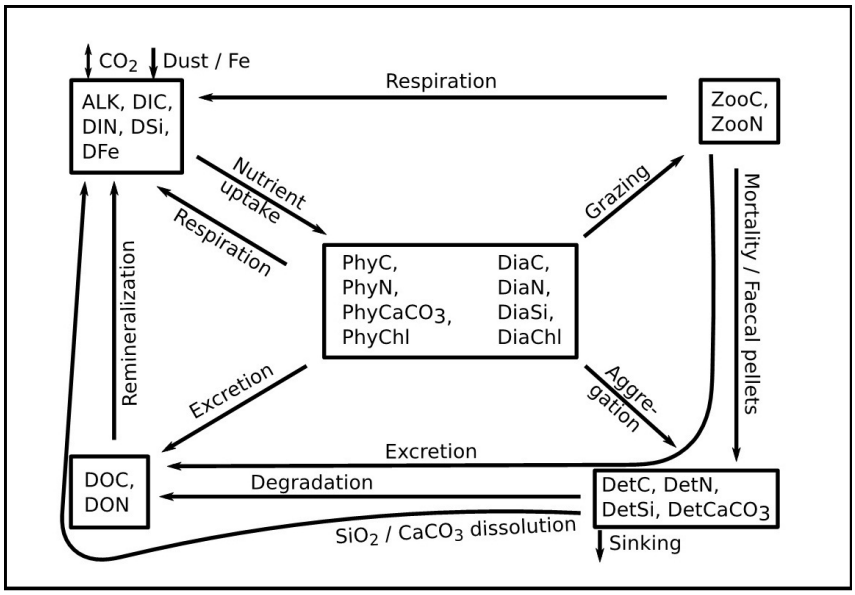

Figure 3: *Schematic sketch of the REcoM ecosystem model. Sources and sinks are shown by arrows. Short arrows denote exchange with atmosphere and sediments. [Hauck et al., 2013, supplement]*

dissolved organic matter at a temperature dependent rate. Both biogenic silica and $CaCO_3$ in the detritus also dissolve during sinking at different rate. The sinking speed of detritus increases linearly with depth [Kriest and Oschlies, 2008] and phytoplankton and diatoms particles sinking speed is constant and set to zero in the present setup. Accumulation of sinking material is allowed in one single sediment layer in the model. Remineralisation of organic detritus reduces dissolved organic carbon (DOC) and dissolved organic nitrogen (DON). In the sediment layer, further remineralisation of organic material and dissolution of silica and $CaCO_3$ take place. DIC and TA are the carbon system parameters [Hauck et al., 2013, supplement] as described in section 1.3, and or used to calculate air-sea flux of CO_2.

2.2 Model setup

A nearly global model configuration without the Arctic Ocean is used on a 2° longitude and $\times(0.38$ to $2°)$ latitude grid. In the Southern Hemisphere, the latitudinal spacing is 2° times the cosine of the latitude for a better resolution in the Southern Ocean. The resolution is increased to a half degree around the equator to resolve the equatorial undercurrent [Aumont et al., 1999]. In vertical, the model has 30 layers with thicknesses increasing from 10 m at the surface to

500 m below in a depth of 3700 m [Hauck et al., 2013]. The model is coupled with a thermodynamic and dynamic sea-ice model [Losch et al., 2010]. A parameterization of effects of mesoscale eddies on the mean flow is applied by following [Gent and McWilliams, 1990] while density-driven down-sloping flows on continental shelves are parameterized following [Campin and Goosse, 1999]. The model is integrated from a state of rest over a thousand years. Initialisation of the model is done with the January salinity, temperature, nitrate and silicate fields of the World Ocean Atlas 2009 (WOA09) [Locarnini et al., 2010, Antonov et al., 2010, Garcia et al., 2010] and with mean alkalinity and preindustrial DIC fields [Key et al., 2004]. The initial field for dissolved iron is obtained from PISCES output [Aumont et al., 2003] after applying a correction based on observed profiles [de Baar et al., 1999, Boye et al., 2001] to reduce a high iron bias in the Southern Ocean [Hauck et al., 2013, supplement]. Climatological forcing fields of the Common Ocean-Ice Reference Experiment (CORE) data set are used as atmospheric forcing of the model. The forcing fields are six hourly 10 m winds, 2 m air temperature, humidity and sea level pressure, daily downward long and short wave radiation fields and monthly precipitation [Large and Yeager, 2004]. The concentration of CO_2 in the atmosphere is prescribed, but varies in time over the course of a model integration, following the observed trend over the period from year 1000 to 2000.

2.3 $CaCO_3$ formation and dissolution in the model

In REcoM, the production of biogenic $CaCO_3$ is limited to phytoplankton and is strictly proportional to the growth of the small phytoplankton model compartment. It is assumed that a constant fraction of the small phytoplankton consists of coccolithophores which have a constant $CaCO_3$: organic carbon ratio. Formation of $CaCO_3$ by heterotrophs, i.e. organisms that use organic carbon from other organisms as food such as foraminifera or pteropods is neglected. Calcification is therefore proportional to gross carbon fixation by nanophytoplankton. For the purpose of the study a second parameterisation is used which is taken from [Aumont and Bopp, 2006] where the proportionality between Gross Primary Production (GPP) of nanophytoplankton and calcification is modulated by a dependency on temperature, nutrient availability and biomass. The calcite production ratio includes the ratio of $CaCO_3$ producers to total nanophytoplankton and the $CaCO_3$: POC (Particulate Organic Carbon) ratio in coccolithophorids and it is assumed to be 0.02 in the standard model setup. As shown in figure (3), the transformation of

biogenic $CaCO_3$ into detritus $CaCO_3$ happens whenever small phytoplankton biomass is transferred to zooplankton and detritus during excretion, respiration, aggregation and grazing. The aggregation function is assumed to be proportional to the abundance of phytoplankton and detritus. The specific aggregation rates are constants for phytoplankton and detritus, which reflect the roles of phytoplankton and detritus in the aggregation process [Hauck et al., 2013, supplement]. Grazing is implemented as a sigmoidal function of prey density [Gentleman et al., 2003]. The contributions of grazing on nanophytoplankton and on diatoms to the total grazing flux are calculated by their respective proportion to the total zooplankton food resource. They are calculated in units of nitrogen biomass and converted to $CaCO_3$ using the intracellular $CaCO_3$: N ratio [Hauck et al., 2013, supplement]. $CaCO_3$ in the detritus sinks together with the rest of the detritus at the same vertically increasing sinking speed. Doing so, it is subject to dissolution. At present in the model, dissolution does not depend on saturation. Instead it is described as a first order process with a temperature dependent dissolution rate. The dissolution rate is constant in such a way that the variation vertical flux of calcite scales with a vertical length scale of 3500 m [Yamanaka and Tajika, 1996].

3 Analysis of model output

After integration of the model over a thousand years, the model results were plotted using MATLAB. First, alkalinity is analysed. Alkalinity is strongly affected by formation and dissolution of $CaCO_3$ and at the same time there exist enough observations, so that the distribution from model output can be compared with them. Unlike DIC, which is also affected by calcification, TA is only weakly affected by net primary production (NPP) and has no gas exchange. The model uses the gridded GLODAP observations (climatology) [Key et al., 2004] of alkalinity as initial conditions. These are as taken as the best representation of real observations, for the purpose of this analysis.

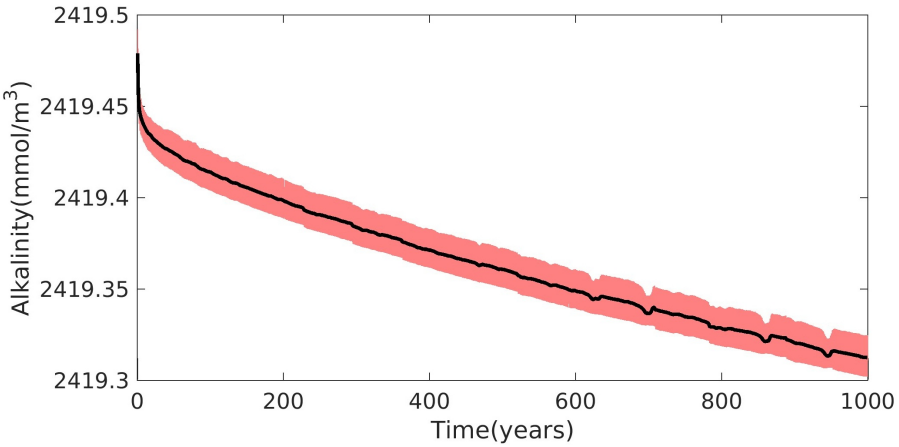

Figure 4: *Decrease of global mean alkalinity over 1000 years model integration; The black solid line represents mean average alkalinity decrease in the global ocean and red color represents the seasonal cycle.*

It is seen from figure (4) that, the globally averaged alkalinity decreases slightly by about less than 0.18 mmol/m^3 over the course of the model integration. When the integration starts, the ecosystem model produces calcite that sinks. As long as it sinks it is still in the form of calcite and taken out of alkalinity. That is why alkalinity initially is reduced quickly. Part of this calcite sinks in the bottommost ocean layer and accumulates there. Compared to the global averaged alkalinity of more than 2400 mmol/m^3, the decrease is small and indicates that the accumulation of $CaCO_3$ in the sediments does not provide a large sink of alkalinity in the model.

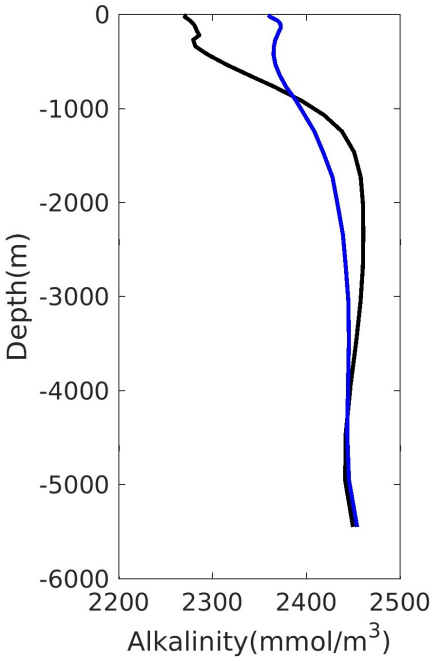

Figure 5: *Global average vertical profile of alkalinity; blue line denotes initial (1000 years before) and black line denotes the final alkalinity profile, averaged over the last model year.*

Figure (5) shows the globally averaged vertical profile of alkalinity from the beginning and the end of the integration. From the profile, it is observed that, the initial conditions are relatively homogeneous. Surface alkalinity concentration decreases by about 100 mmol/m^3 over the course of the integration whereas it increases between 1000 m to 4000 m depth. The strongest increase in alkalinity is observed between 1200 m to 2000 m depth. The model has therefore shifted too much alkalinity from the surface into layers between 1000 m to 4000 m depth.

Figure (6) displays the global surface alkalinity distribution and the differences between beginning and end over a thousand years time period in the ocean. It is clearly observed from figure (6) that, compared to the initial conditions at the surface alkalinity decreases more or less everywhere within the oceans. There are massive reductions in the subtropical South Atlantic and Pacific of about 200 to 300 mmol-eq/m^3 and a slight decrease in the Indian Ocean. Alkalinity decreases strongly within the region from 30° N to 30° S globally. The pattern that alkalinity is highest in the subtropics and higher in the Atlantic than in the Pacific, however is still visible in the final distribution. An unrealistic increase in alkalinity is observed near the

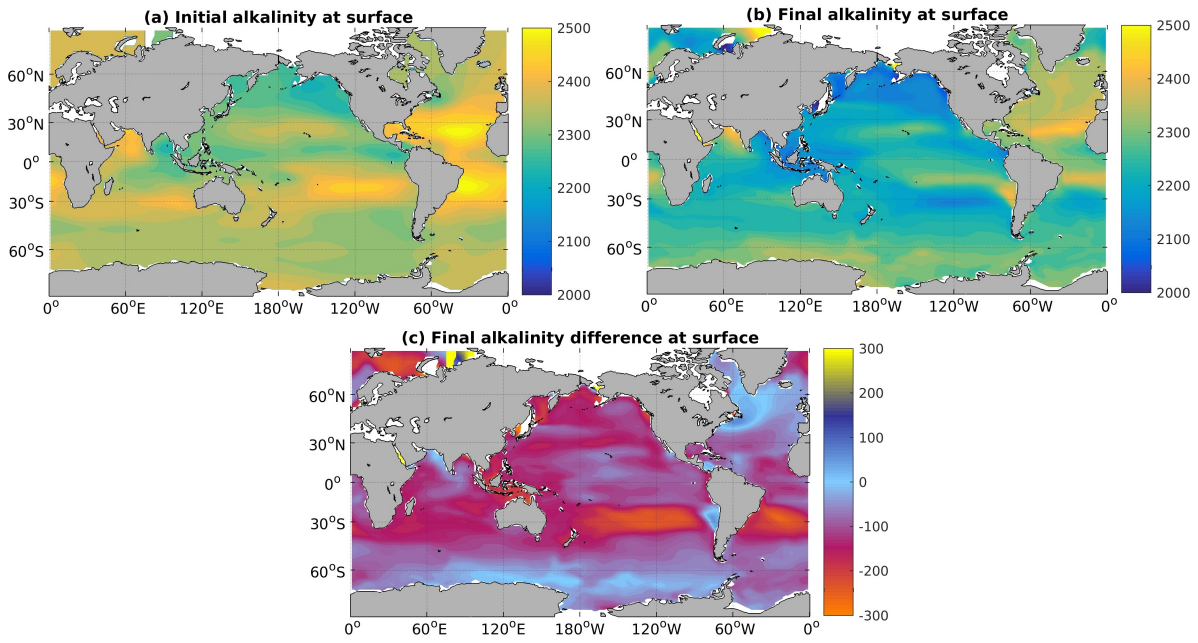

Figure 6: *Global distribution changes of alkalinity at the ocean surface over 1000 years of integration; initial alkalinity distribution in the ocean surface denoted by (a) whereas (b) denotes after 1000 years; The surface alkalinity difference over 1000 years integration time in the ocean is denoted by (c). A different colourbar is used for the alkalinity difference.*

kara sea perhaps caused by the weak circulation in this part of the ocean model, caused by the closed boundary at 80° N and the shallow water depth. In addition, the freshwater input into the Arctic has been redistributed in the model over the closed boundary at 80° N.

The main factors affecting alkalinity at the surface are freshwater fluxes (evaporation, precipitation and river run-off) and calcification. The decrease of alkalinity could therefore be connected to either a too strong freshwater input in the surface or a too strong calcification.

Since the model conserves alkalinity almost exactly, the decrease of alkalinity at the surface must be accompanied by an increase at depth. The maximum alkalinity increase is found in 1730 m depth within the water column which corresponds to layer 21 (1730 m depth) within the 30 model layers.

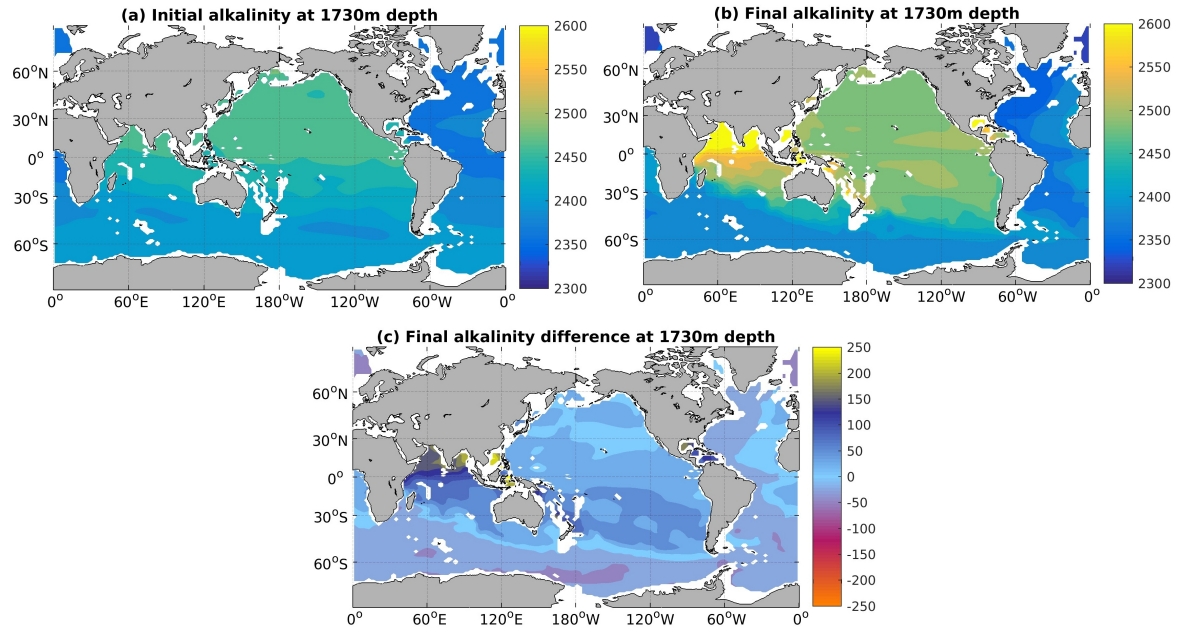

Figure 7: *Global distribution changes of alkalinity at 1730 meter depth in the ocean over 1000 years of integration; initial alkalinity distribution in 1730 m depth denoted by (a) whereas (b) denotes after 1000 years; alkalinity difference over 1000 years integration time in the ocean is denoted by (c).*

Figure (7) shows the result of this shift of alkalinity from the surface into mid layers in the ocean. While surface alkalinity decreases everywhere in the ocean, increases at depth are stronger in the deep Pacific and Indian ocean. One possible explanation could be that the increase is caused by calcite from sinking detritus being dissolved while the water moves with the conveyor belt. The deep Pacific and the Indian Ocean contain the oldest water so that they have the longest time to accumulate alkalinity from dissolution. The second possible explanation for the observed result is that the, the total amount of calcification might be wrong and the model has done therefore a too high dissolution within the water column. To investigate this further, a good way is to look at the POC and $CaCO_3$ export at 100 m depth.

For the organic carbon export shown in figure (8 a), there is a band of high productivity along the equator due to upwelling. Enhanced productivity is also found near Namibia and Mauritania in the Atlantic. The subtropical regions are oligotrophic i.e., nutrient poor so that there is not much export of organic carbon. Enhanced productivity is also detected in the subpolar regions in the Atlantic and the North Pacific, around Antarctica and throughout the north Indian Ocean

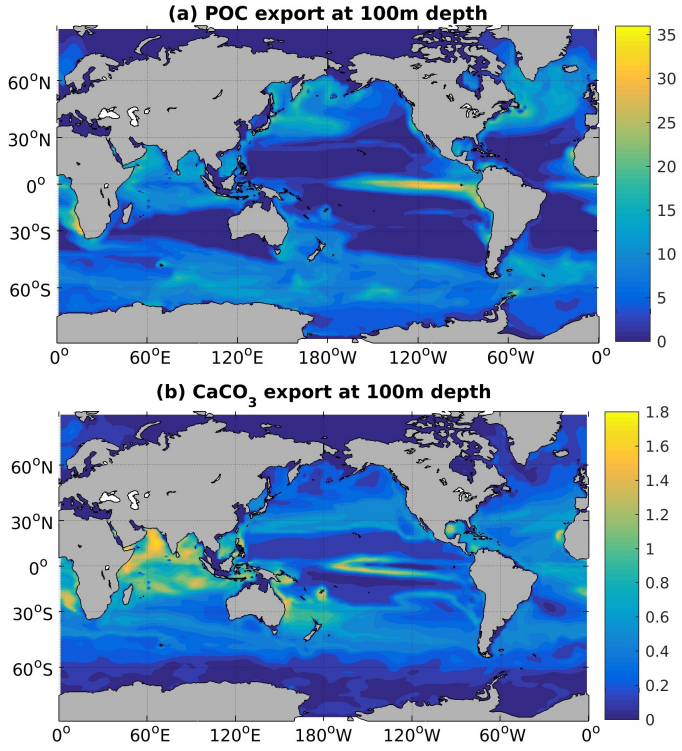

Figure 8: *Total organic carbon export at 100 m depth, (a) Particulate organic matter (POC) and (b) $CaCO_3$; two different colour-bar for better understanding.*

mostly driven by diatoms. The calculated total export of organic carbon is 9.536 Pg C yr^{-1}.

The formation and export of $CaCO_3$ shown in figure (8 b) in the model is driven by small phytoplankton. Due to their higher nutrient uptake affinity but lower maximal growth rate, small phytoplankton has an advantage at lower nutrient conditions, while diatoms dominate when nutrients are abundant. This pattern is reflected in the distribution of $CaCO_3$ export. The maximum export mostly occurs at the boundaries between high nutrient and low nutrient conditions, e.g. at the boundaries of equatorial upwelling; and between 30° N to 40° N and 30° S to 40° S. The subpolar regions, where much POC export happens, are regions of less $CaCO_3$ export. The maximum export of $CaCO_3$ is found in the Indian Ocean. The model calculates a total export of $CaCO_3$ of 0.685 Pg C yr^{-1} which is quite satisfying with respect to the global observations that are in a range between 0.4 and 1.8 Pg C yr^{-1} [Berelson et al., 2007].

4 Experimental Simulation

4.1 Sensitivity experiments varying the calcification ratio

Two experimental model simulations are done to investigate possible causes of the alkalinity shifting from surface to the mid layers by changing the $CaCO_3$ production ratio (CR) which is basically ratio of calcifiers to non calcifiers. In the new experimental sensitivity simulations this ratio is changed from 0.02 mol/mol to 0.01 mol/mol and 0.03 mol/mol.

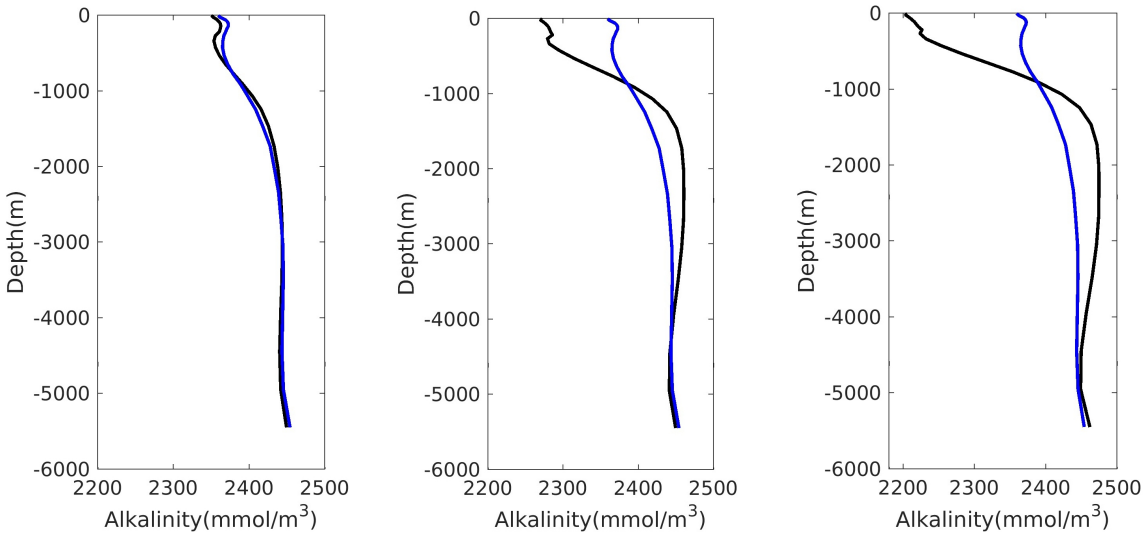

Figure 9: *Global average vertical profile of alkalinity with different calcification ratio; From left to right the order denotes calcification ratios of 0.01, 0.02 and 0.03; blue line denotes initial (1000 years before) and black line denotes the final alkalinity profile.*

Figure (9) shows different global average vertical profiles for alkalinity obtained from the simulations with different CR. For CR = 0.01, the globally averaged vertical profile of alkalinity is much closer to the initial. A slight decrease of alkalinity concentration at the surface is observed which is about 20 mmol/m^3 over the course of the 1000 years integration whereas alkalinity increases between 1000 m to 3000 m depth. A maximum increase of alkalinity is observed between 1000 m to 2000 m depth while a slight decreases of alkalinity concentration is observed from 3000 m to 5500 m depth. From the observation it is clear that, still the model is shifting alkalinity from the surface and bottom ocean to mid layers between 1000 m to 3000 m. On the other hand, the vertical profile obtained from the simulation data with CR = 0.03

shows very high shift of alkalinity from surface to mid layer with a high alkalinity decrease at the surface of about 160 mmol/m^3, is stronger than in the reference run. For further analysis it is needed to look at the global surface distribution and difference in alkalinity.

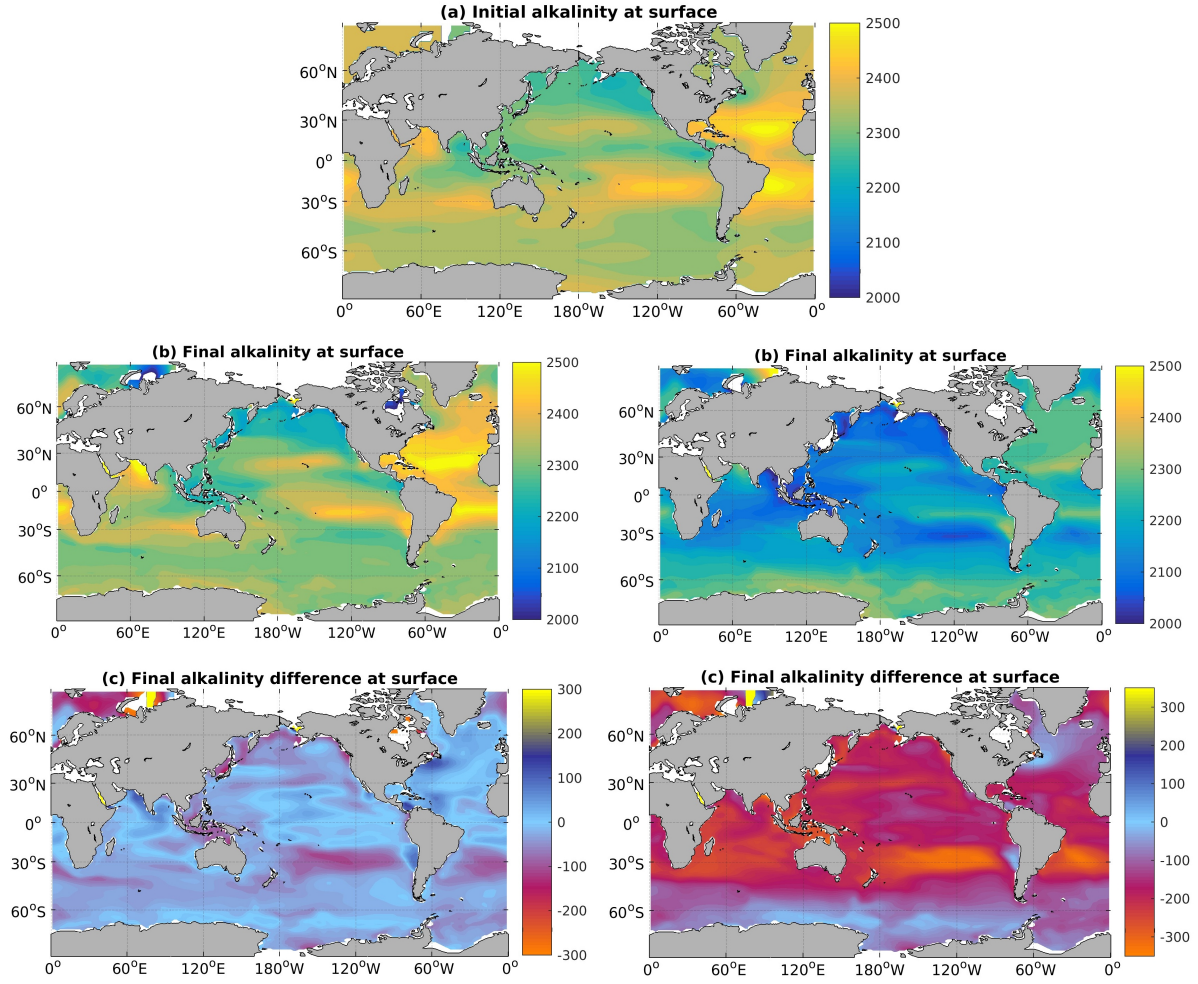

Figure 10: *Global distribution changes of alkalinity at the ocean surface over 1000 years of model integration time with different calcification ratios; Left column of images represent the outcome of the model simulation with a calcification ratio 0.01 and the right column represents CR = 0.03. The initial alkalinity distribution in the ocean surface before 1000 years denoted by (a) whereas (b) denotes after 1000 years; surface alkalinity differences over a 1000 years in the ocean is denoted by (c). A different colourbar is used for alkalinity difference.*

Figure (10) represents the global surface distribution of alkalinity and alkalinity difference after an integration of the model over 1000 years with CR = 0.01 and 0.03 respectively. From figure (10) with CR = 0.01, it is clearly seen that, compared to the initial conditions at the

surface alkalinity decreases slightly but not uniformly. In the Pacific, an increase is observed in a range between 0° to 30° N about 20 mmol/m^3 whereas decrease in alkalinity is observed almost everywhere in a range from 0 mmol/m^3 to 35 mmol/m^3 with a maximum decrease near 30° S. About 50 mmol/m^3 of increase in alkalinity is observed over the Indian Ocean and the Bay of Bengal. For CR = 0.03, a very strong shifting of alkalinity from surface to mid layer depth is observed in a wide range between 10 mmol/m^3 to 300 mmol/m^3 through all over the global oceans because of much calcification is done by the model. The next step is to look at the mid layer alkalinity at 1730 m depth.

Since the model conserves more or less alkalinity, any decrease of alkalinity at the surface must be accompanied by an increase at depth. From figure (11) with CR = 0.01, it is clearly observed that, the model is not shifting much alkalinity from the surface to the mid layer depth. There are some increases in alkalinity over the Northern Indian Ocean along with the Bay of Bengal and over a portion of the North Atlantic between 45° N to 60 ° N. The approximate range of increase over those areas is between 10 mmol/m^3 to 20 mmol/m^3. There are more or less no changes in alkalinity in between 0 ° S to 50 ° S but decrease of about 12-15 mmol/m^3 is observed in the Southern Ocean and in the North Pacific. On the other hand, the model output with CR = 0.03 exhibits a strong alkalinity shift from surface to 1730 m depth with a pattern that is similar to the reference run but with a higher amplitude.

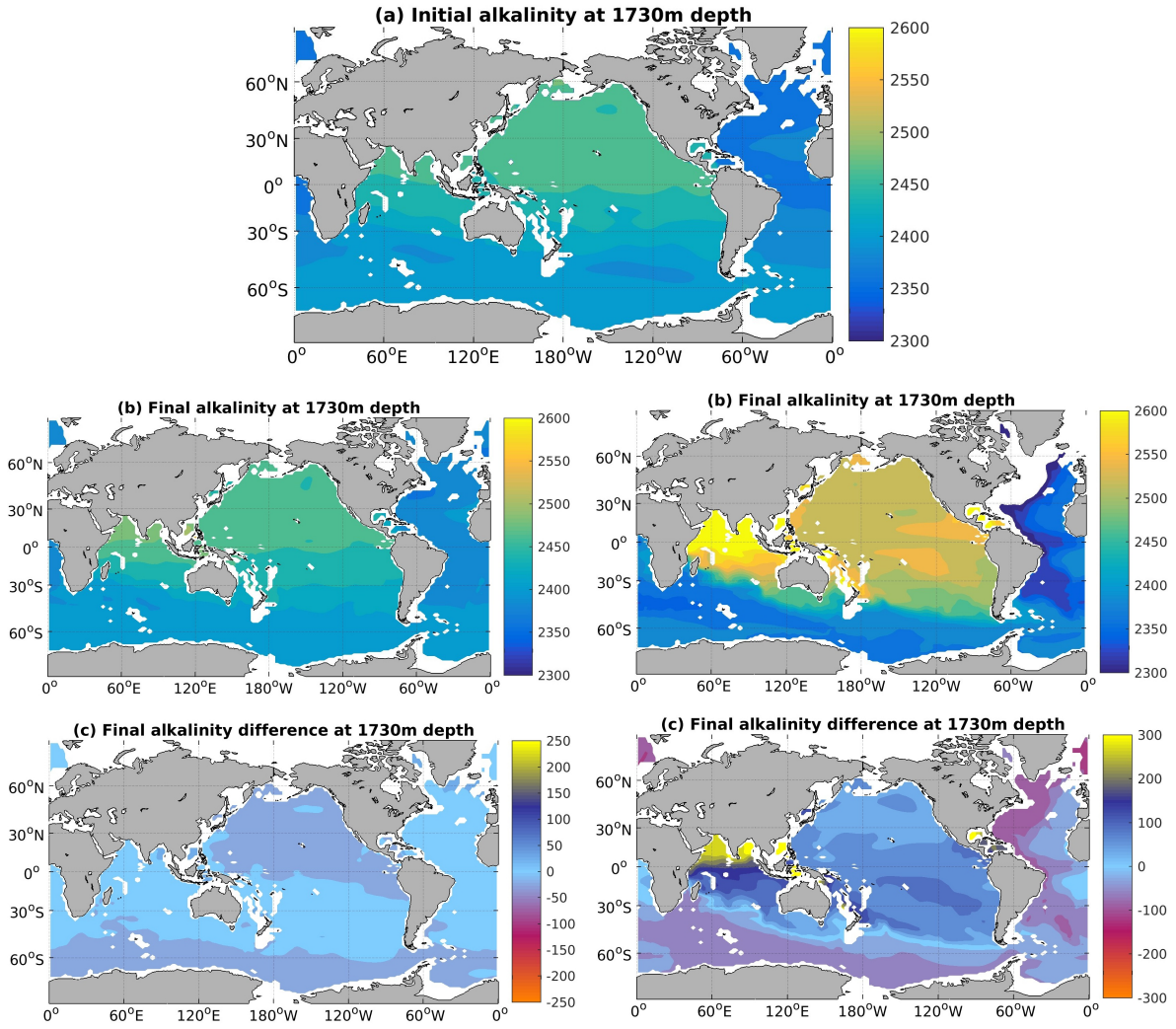

Figure 11: *Global distribution changes of alkalinity at 1730 meter depth in the ocean over 1000 years of model integration time with different calcification ratios; The left column of images represent the outcome of model simulation with calcification ratio 0.01 and the right column represents CR = 0.03. The initial alkalinity distribution in the 1730 m depth before 1000 years denoted by (a) whereas (b) denotes after 1000 years; alkalinity differences over a 1000 years in the ocean is denoted by (c). A different colourbar is used for alkalinity difference.*

To continue with the model simulation with calcification ratio 0.01, next step would be to look at the POC and $CaCO_3$ export at 100 m depth.

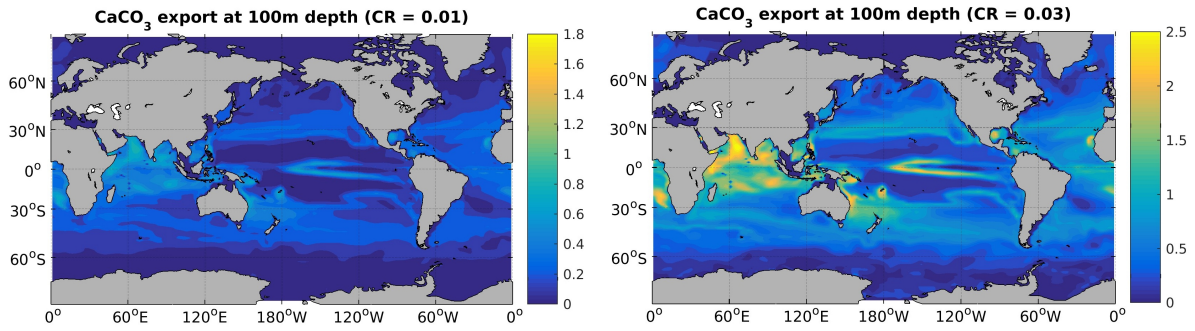

Figure 12: *Total $CaCO_3$ export at 100 m depth with different calcification ratio; From left to right images represents model simulation with CR = 0.01 and 0.03 respectively. A different colourbar is used for better understanding.*

For both sensitivity simulation with CR = 0.01 and 0.03, organic carbon export pattern is identical because the calcification ratio of the model has no effect on POC export so that the model conserves the amount of particulate organic carbon export of 9.536 Pg C yr^{-1}. A visualization of POC export is already shown in the previous chapter for reference run.

While organic carbon export is equal for different CR, $CaCO_3$ export is different for different calcification ratio. The formation and export of $CaCO_3$ shown in figure (12) in the model is driven by small phytoplankton. The maximum export mostly occurs at the boundaries between high nutrient and low nutrient conditions, e.g. at the boundaries of equatorial upwelling; and between 25° N to 40° N and 25° S to 40° S. The subpolar regions, where much POC export happens, are regions of less $CaCO_3$ export. The maximum export of $CaCO_3$ is found in the Indian Ocean. The model calculates a total export of $CaCO_3$ of 0.343 Pg C yr^{-1} for CR = 0.01.

On the other hand, the export of $CaCO_3$ for model simulation with CR = 0.03 is higher than in the previous model simulation (12), may be a bit unrealistic because of high export value. A wide band of high productivity is observed more or less in a range between 30° N to 30° S because of strong calcification in the high nutrient boundaries. For the higher calcification ratio, the model calculates the total export of $CaCO_3$ of 1.028 Pg C yr^{-1}.

4.1.1 Basinwise analysis

Along with $CaCO_3$ production and dissolution, the surface distribution of alkalinity in the ocean is also affected by precipitation and evaporation [Millero et al., 1998]; riverine inputs of alkalinity [Cai et al., 2010, Friis et al., 2003]; upwelling of high alkaline subsurface waters resulting from dissolution of $CaCO_3$ [Lee et al., 2006] and by biological productivity [Wolf-Gladrow et al., 2007]. For a better understanding of the surface distribution of alkalinity the next step is therefore an analysis of process contributions of evaporation, precipitation and river discharge on the ocean alkalinity distribution.

The analysis of alkalinity distribution is done basinwise in this study, following [Fry et al., 2015]. This analysis is performed here only for the reference run with a $CaCO_3$ production ratio (or CR) 0.02 and for the sensitivity model run with CR = 0.01. These two sensitivity simulations are taken to account for different reasons. The reference simulation (CR = 0.02) is the presently used setup of the model and represents present scenario between the model and the global observation. On the other hand, the simulation with CR = 0.01 provides us a better scenario for globally averaged vertical profile, surface distribution and mid layer depth distribution of alkalinity compared to the reference model run. The sensitivity study with CR = 0.01 on the other hand has a quite low global export of $CaCO_3$.

The freshwater flux effect (evaporation, precipitation and river discharge) was quantified based on salinity. Figure (13 a, b and c) shows the surface ocean alkalinity distributions within the Atlantic, Indian and Pacific basins as a function of latitude. All three basins from (13 a, b and c) exhibit local maxima of alkalinity arround 30° N and 20° S which are the centres of subtropical gyres. These maxima are result of the hydrological cycle driving substantial excess of evaporation over precipitation in these areas. Net evaporation concentrates substances dissolved in seawater and net precipitation dilutes seawater [Fry et al., 2015]. As alkalinity is a weighted sum of different dissolved constituents, it is proportional to salinity concentration [Zeebe and Wolf-Gladrow, 2001, chapter 1, p.29]. A salinity normalization on alkalinity (Alk_1) is then done to remove the effect of evaporation and precipitation (i.e.,the hydrological cycle effect) by converting each alkalinity (Alk) measurement to its expected value at a salinity (S) of 35 using equation (4) [Postma, 1964, Millero et al., 1998].

$$\mathrm{Alk}_1 = \frac{\mathrm{Alk} \times 35}{\mathrm{S}} \tag{4}$$

In this analysis, the model output is compared with the output from [Fry et al., 2015] as global observations to investigate basinwise alkalinity distribution (Alk) and salinity normalized alkalinity (Alk_1).

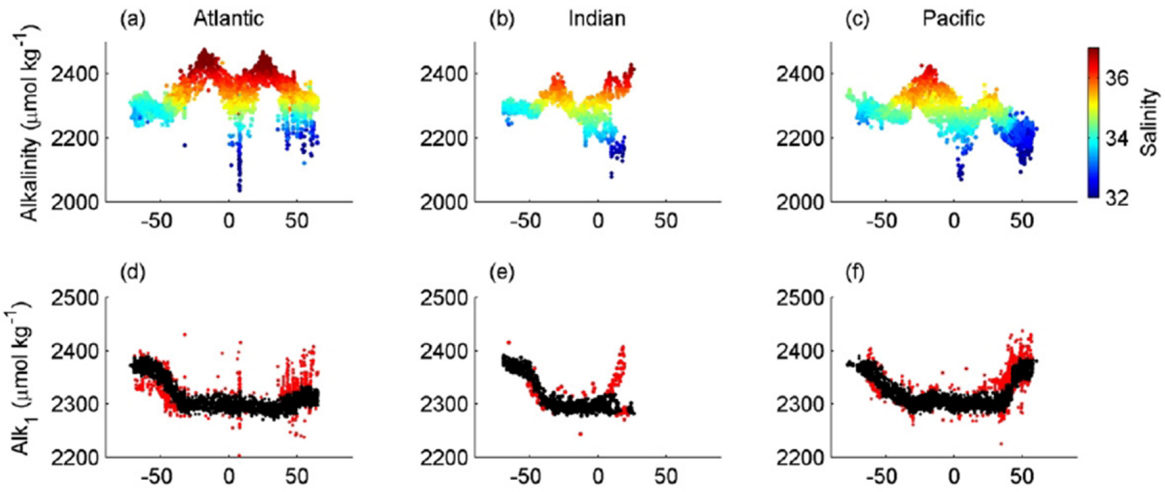

Figure 13: *The distribution of alkalinity (Alk) and normalized alkalinity (Alk_1) in the three major ocean basins. a, b and c show the observed alkalinity with colours indicating the salinity. d, e and f show alkalinity with salinity normalization (Alk_1). The red points indicating values more than 20 μ*mol kg^{-1} *over the 5° of latitude running mean. [Fry et al., 2015]*

Both simulations of the model reproduce the general pattern of elevated alkalinity in the center of the subtropical gyres. In the simulation with CR = 0.02, low alkalinity (Alk) below of 2300 μmol kg^{-1} is observed around the equator (fig. 14 a) in the Atlantic compared to global observation. A lower alkalinity (Alk) is observed over 30° S of about 70 μmol kg^{-1} in the Atlantic. For the Indian Ocean, lower alkalinity (Alk) is observed for CR = 0.02 throughout the global oceans (fig. 14 b) due to much calcification and dissolution by the model. For the Pacific, model output (fig. 14 c) shows decreased alkalinity (Alk) value compared to the global observations with high value in lower lattitude and lower in high lattitude. Compared to figure (13), the observed Alk (fig. 14 a, b and c) exhibits a north-south asymmetry in the distribution in the Atlantic and in the Indian Ocean.

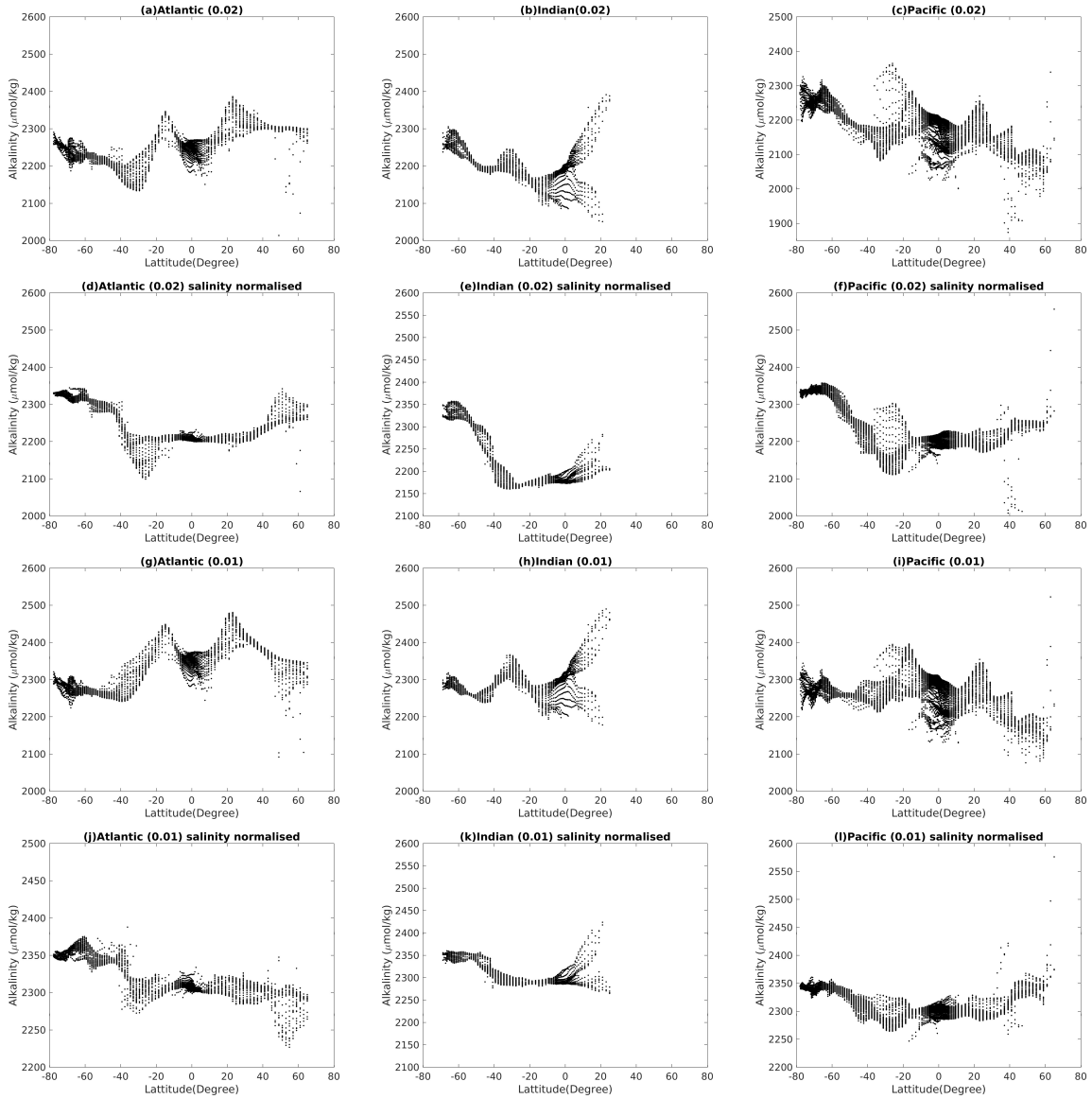

Figure 14: *The distribution of alkalinity (Alk)* (μmol kg^{-1}) *and normalised alkalinity (Alk$_1$) in the major Ocean basin. (a, b, c) shows the Alk distributions for model simulation of 1000 years integrated time with CR = 0.02, (d, e, f) denotes salinity normalized alkalinity (Alk$_1$) with CR = 0.02, (g ,h, i) shows alkalinity (Alk) distribution with CR = 0.01 and (j, k, l) shows salinity normalised alkalinity (Alk$_1$) distribution with CR = 0.01.*

After the salinity normalization on modeled (CR = 0.02) alkalinity data, a lower Alk_1 figure (14 d) is observed compared to figure (13) in the Atlantic. The decreases are maximal over 30° S (subtropic) of about 200 μmol kg^{-1} and minimal over the areas between 50° S and 50° N of about 30 μmol kg^{-1}. The overall alkalinity (Alk_1) distribution of the Atlantic shows deficiencies compared to (fig. 13). For the Indian Ocean (fig. 14 e) compared to figure (13), a massive decrease in Alk_1 of about 150 μmol kg^{-1} is observed over a vast area in between 40° S to 20° N. For the Pacific, modelled global pattern of alkalinity (Alk_1) (fig. 14 f) still looks having deficiency of about 60-100 μmol kg^{-1} compared to figure (13). For the three ocean basins, Alk and Alk_1 profiles show defficiency in alkalinity which is maximal in the Atlantic and minimal in the Pacific. A lower difference is observed for Alk_1 (fig. 14 d, e and f) between the Southern Ocean and low latitudes compared to figure (13 d, e and f) for modelled data with CR = 0.02.

For the sensitivity simulation with CR = 0.01, overall alkalinity (Alk) distribution for the Atlantic (fig. 14 g) looks much better compared to simulation with CR = 0.02. A deficiency in alkalinity (Alk) in the lower lattitudes is observed compared to figure (13 a). For the Indian Ocean (fig. 14 h), model output with CR = 0.01 shows almost similar alkalinity pattern compared to figure (13 b) but with a slight decrease of approximately 10 - 20 μmol kg^{-1} throughout the whole ocean basin. For the Pacific (fig. 14 i), model output with CR = 0.01 shows much better alkalinity (Alk) than the previous one (CR = 0.02) compared to figure (13 c). A decrease in Alk is observed in the North Pacific of about 30 μmol kg^{-1}.

After the salinity normalization on simulation data (CR = 0.01), overall alkalinity (Alk_1) distribution of the Atlantic (fig. 14 j) shows slightly lower value compared to figure (13 d) while regions between 40° N and 60° N has a bit lower value. For the Indian Ocean (14 k), salinity normalized alkalinity (Alk_1) distribution shows a better result with a little deficiency in of about 20 - 30 μmol kg^{-1} in lower latitudes. For the Pacific (fig. 14 l), Alk_1 pattern looks much flatter in between 60° S to 40° N while decreases are observed in lower and higher latitudes. Decreases in Alk_1 (fig. 14 j, k and l) are observed in between the Southern Ocean and lower latitude compared to figure (13). The deficiencies in Alk_1 in the Atlantic is of about 50 μmol kg^{-1} while about 10 μmol kg^{-1} are observed the Indian and the Pacific respectively.

A prominent feature that is seen both in the global observations and in the model run is that there is a split in the Alk - latitude relationship in the Northern Indian Ocean. This is partly

caused by salinity differences between the Arabian Sea and the Bay of Bengal. But also the normalising alkalinity of the riverine inflow towards the Bay of Bengal plays a role [Fry et al., 2015]. The model is able to reproduce this pattern at least qualitatively.

Modelled alkalinity (both Alk and Alk_1) distribution for the both simulations show deficiences in the Southern Ocean compared to the observations except the Indian Ocean (fig. 14). A possible explanation for this is that the circumpolar deep water has a too low alkalinity. The Southern Ocean is a region of upwelling where the circumpolar deep water flow reaches to the ocean surface carrying lower alkalinity. The model dissolves $CaCO_3$ with a constant rate everywhere in the ocean. But there are differences in the dissolution of $CaCO_3$ in the global oceans especially in the Pacific and the Atlantic. In the Pacific, the dissolution depth is shallower because of higher dissolved carbon value while in the Atlantic dissolution occurs mostly in the deep water. This is not reflected in the model.

4.2 Experiment with modified calcite equation

After having the output from the model and analysing the plots, it is necessary to make new experimental simulation with a new model setup which has temperature dependent calcification to non calcification ratio as well as biomass and nitrogen limitation on Coccolithophores. The rain ratio in reality is not constant, and it makes sense to investigate further whether a variable ratio between calcification and POC production by small phytoplankton could give more realistic results. These parameterisations are mainly based on the assumption that there is a constant ratio of $CaCO_3$ production to primary production of small phytoplankton clearly simplistic from [Zondervan, 2007]. It is known that Coccolithophores are not very abundant neither in very oligotrophic waters nor in very low temperature; calcification reaches at maximum at intermediate light level zone while decreases at either low light level or high light levels; Coccolithophores are present at stratified water and grows maximum in mid-lattitudes in approx temperature of 10° C. Some models therefore make the $CaCO_3$: POC production ratio dependent on variables like temperature, nutrient concentration etc [Aumont and Bopp, 2006, supplimentary material]. The parameterisation of new sensitivity runs with the model is following the PISCES model which describes this ratio by:

$$\mathrm{R}_{CaCO3} = \mathrm{R}^{*}_{CaCO_3}\mathrm{L}^{\mathrm{N}}_{\mathrm{lim}}\max(0.0001, \tfrac{\mathrm{T}}{2+\mathrm{T}})\max(1, \tfrac{\mathrm{p}}{2}) \tag{5}$$

In equation (5), the ratio between $CaCO_3$ formation and POC production in small phytoplankton is dependent on the nitrogen limitation term L^{N}_{lim}, which varies between 0 (for nutrient-limiting conditions) and 1 (for abundant nutrients), local temperature T in degree celcius and small phytoplankton biomass P in mmol Nitrogen/m^3 (mmol N/m^3).

In this experiment, calcification ratio (CR) has been changed in to $\mathrm{R}^{*}_{CaCO_3}$ for new parameterized calcite equation. Four new simulation is done with the calcification ratio (CR) 0.01, 0.02, 0.03 and 0.04 over a 1000 years of model integration time named as Exp 03, Exp 04, Exp 05 and Exp 06 consicutively. To validate the parameterisation based on assumption, first step would be to analyse the global average vertical profile of alkailinity.

Figure (15) shows vertical distribution of alkalinity compared to the initial state. From figure (15), it is clearly seen that model simulation with CR 0.01 (Exp 03) exhibits better result

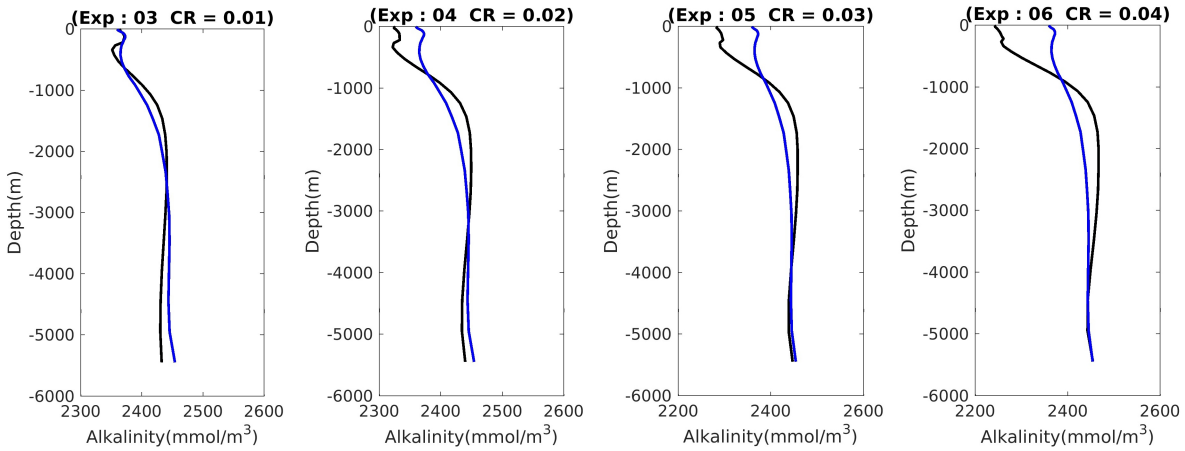

Figure 15: *Global average vertical profile of alkalinity with modified calcite equation for different calcification ratio and modified calcification equation; From left to right the order denotes CR = 0.01, 0.02, 0.03 and 0.04; blue line denotes initial (1000 yeras before) and black line denotes the present alkalinity profile.*

than the others. For Exp 03, strong shift is happening in the surface of the ocean as well as in the mid layed depth. Alkalinity is shifted from 300-500 m from the ocean surface to 900-2200 m depth while a defficiency is observed from 3000- 5500 m depth. On the other hand, the remaining three model runs (Exp 04, Exp 05 and Exp 06) exhibit much more transfer of alkalinity to the deep ocean which is unrealistic. The average mean profile of alkalinity from the different model simulations exhibits huge variations in the vertical distribution of alkalinity throughout the global oceans. The variation increases with calcification ratio. To get a better understanding on how these changes are distributed spatially, next step would be to look at the surface distribution of alkalinity in the ocean.

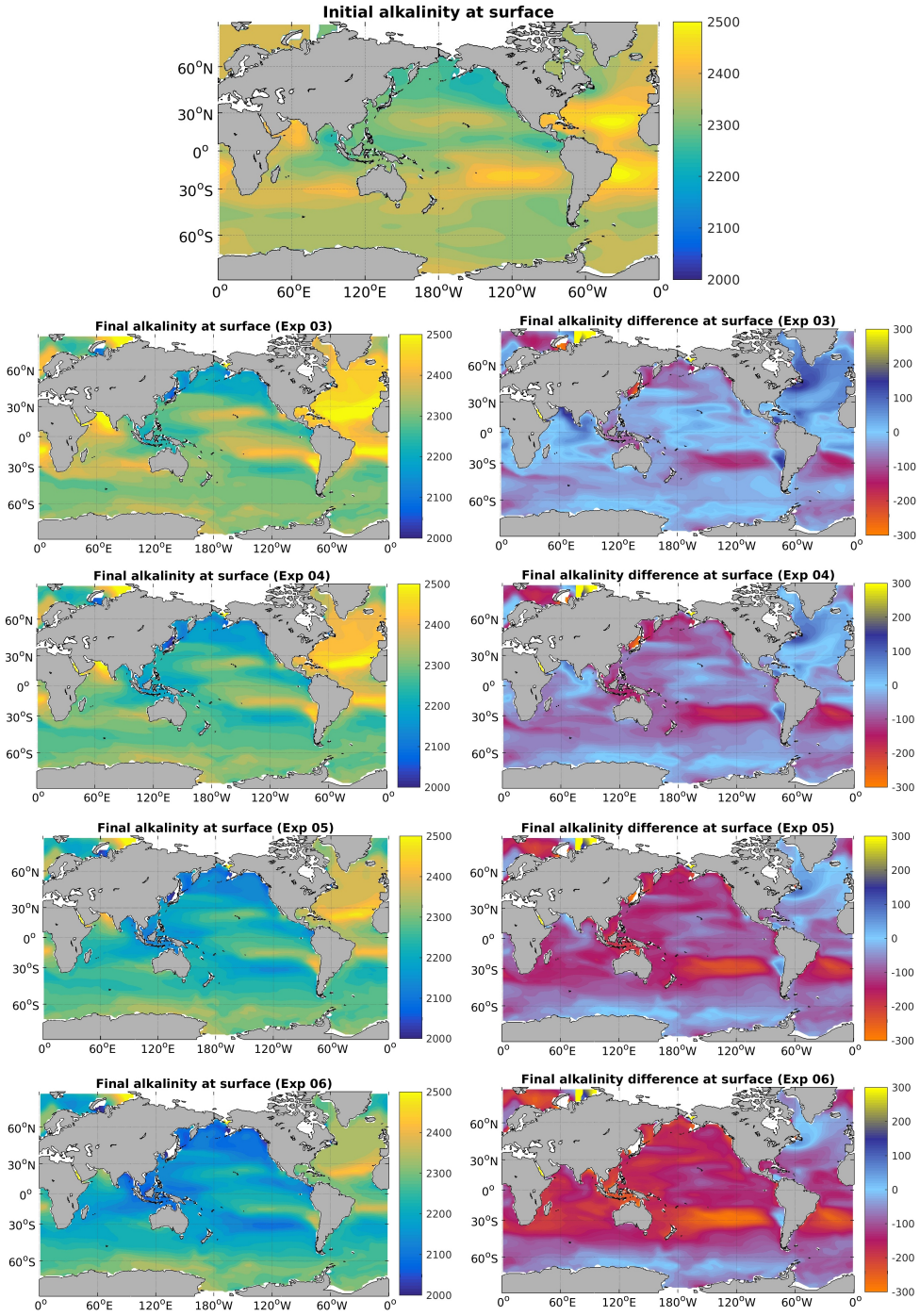

Figure 16: *Global distribution changes of alkalinity at the ocean surface over 1000 years of model integration time with modified calcite equation for Exp 03, Exp 04, Exp 05 and Exp 06; The topmost image represents the initial alkalinity distribution in the ocean surface before 1000 years, the left column images represent the final alkalinity distribution after 1000 years and the right column of images represent surface alkalinity differences over a 1000 years in the ocean. A different colourbar is used for the alkalinity difference for better understanding.*

Figure (16) shows the distribution of alkalinity and the differences between initial condition and after 1000 years at surface in the ocean for Exp 03, Exp 04, Exp 05 and Exp 06. As it is seen that Exp 03 provides better vertical profiles among all these four sensitivity experiment, it would be a wise decision to look at the ocean surface distribution of alkalinity for Exp 03. In the plot for Exp 03, decrease in alkalinity at surface in the ocean is observed more or less everywhere except in the North Atlantic, northern part of the Indian Ocean and in the subtropical Pacific. For the Pacific, alkalinity decreases in a wide range up to 130 μmol kg^{-1} and an increase is observed in 0° to 30° N of about 30 μmol kg^{-1}. For the Atlantic, strong decreases and increases in alkalinity are observed. the Southern part of the Atlantic exhibits strong decrease of about 130 μmol kg^{-1} while an even stronger increase is observed from 15° S to 70° N up to 150 μmol kg^{-1}. For the Indian Ocean, decreases in alkalinity are observed in southern region in a range upto 30 μmol kg^{-1} while a strong increase observed in the north Indian Ocean along with Bay of Bengal of about a range up to 120 μmol kg^{-1}. About a 50 μmol kg^{-1} decrease in alkalinity is observed in the Southern Ocean. For the other sensitivity experiments (Exp 04, Exp 05 and Exp 06) with a higher calcification ratio, the final surface distribution of alkalinity becomes more and more unrealistic. These runs are therefore not considered for further analysis. Since the model conserves alkalinity, an overall decrease of alkalinity at the ocean surface must be compensated by an increase at mid layer depth, or viceversa.

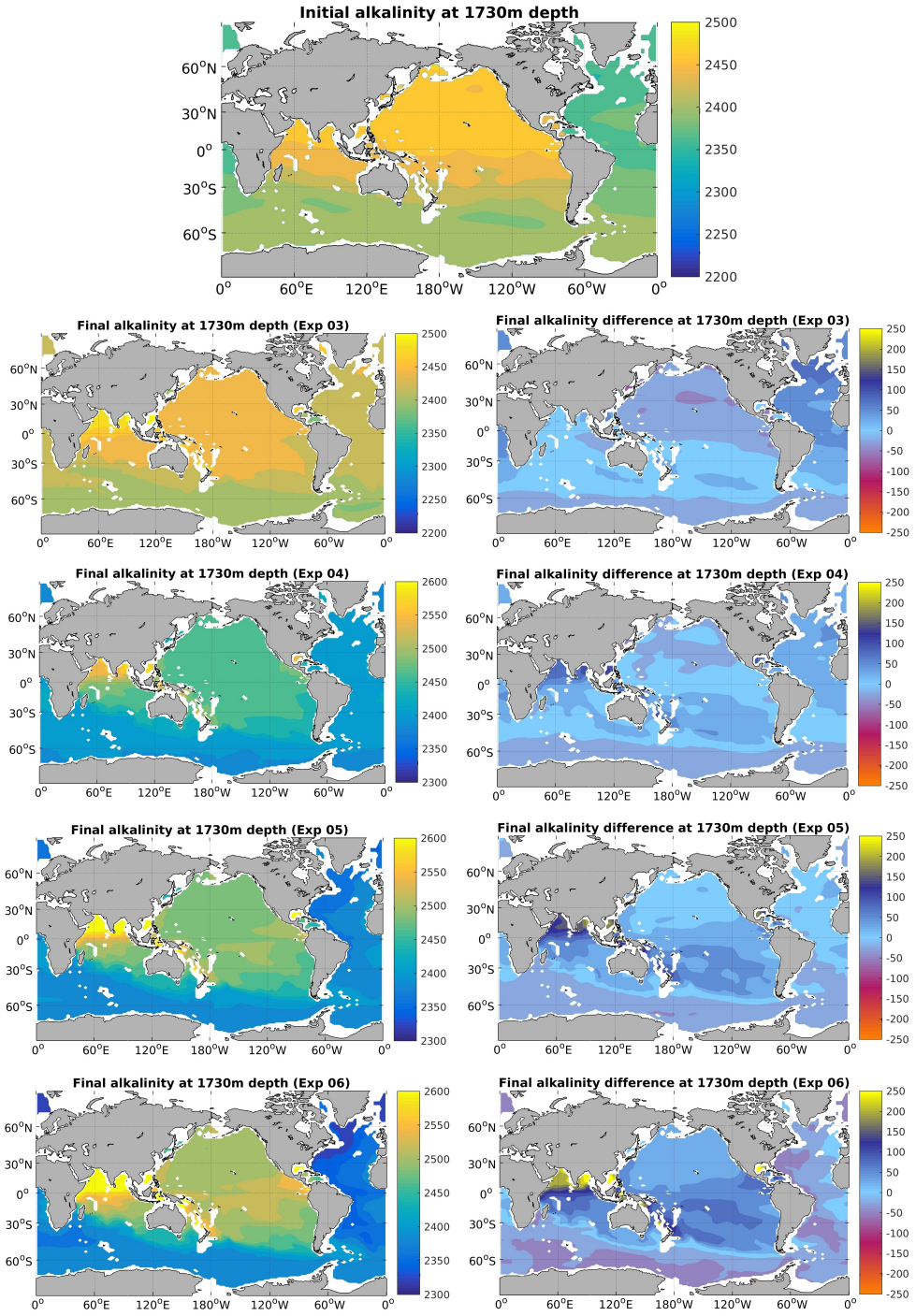

Figure 17: *Global distribution changes of alkalinity at 1730 meter depth in the ocean over 1000 years of model integration time with modified calcite equation for Exp 03, Exp 04, Exp 05 and Exp 06; The topmost image represents the initial alkalinity distribution, the left column images represent the final alkalinity distribution and the right column of images represent alkalinity differences over 1000 years. A different colourbar is used to show alkalinity difference for better understanding.*

Figure (17) represents the global distribution of alkalinity and the changes of alkalinity at 1730 m depth in the ocean for Exp 03, Exp 04, Exp 05 and Exp 06. Following further analysis of Exp 03, the final distribution of alkalinity at 1730 m depth shows an increase of alkalinity in a minimal range up to 40-50 μmol kg^{-1} along the southern subtropical regions of about 0° S to 60° S. For the Pacific, a decrease in alkalinity is observed in its northern part of a range up to 20-30 μmol kg^{-1} while an increase is observed in the South Pacific. In the Atlantic, an increase in alkalinity happens everywhere in a wide range of about 10-50 μmol kg^{-1}. A slight increase is observed over the Indian Ocean along with the Bay of Bengal which is mostly less than 20 μmol kg^{-1}. Final alkalinity distributions from Exp 04, Exp 05 and Exp 06 exhibit unrealistic scenerios and are not considered for further investigations. To analyse more, the next step would be to look at export of $CaCO_3$ at 100 m depth in the ocean.

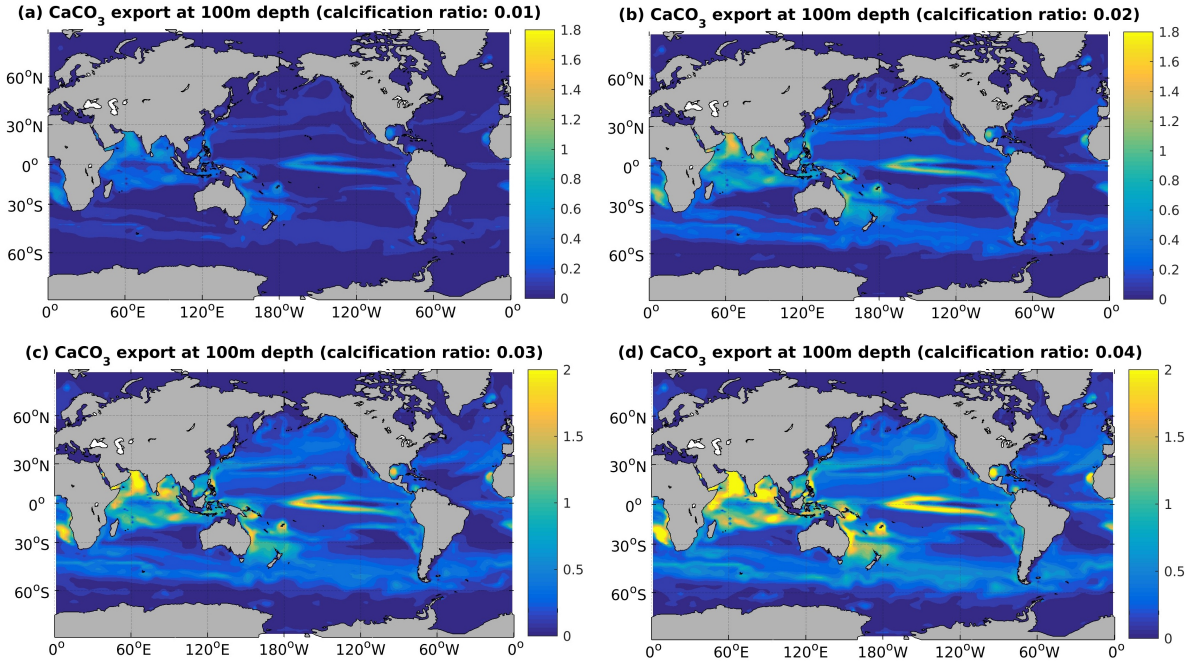

Figure 18: *Total organic carbon export at 100 m depth with modified calcite equation for different calcification ratio.*

Figure (18) represents global distribution of $CaCO_3$ export at 100 m depth in the ocean with different CR. In the model, production and export of $CaCO_3$ is driven by small phytoplankton that have higher nutrient uptake capacity but with a lower maximal growth rate. For a lower nutrient condition, small phytoplankton has an advantage while nutrient abundant conditions

are mostly dominated by diatoms. This mechanism is well reflected in the distribution pattern of $CaCO_3$ export in the ocean.

Figure (18 a) denotes the distribution of $CaCO_3$ (with CR = 0.01) export in the global ocean at 100 m depth. Maximum export is observed at the boundaries of equatorial upwelling, between between between 25° N to 40° N and 25° S to 40° S ; which are mostly the boundaries between high and low nutrient conditions. The subpolar regions exhibit less $CaCO_3$ export despite being an area of high POC export while the Indian Ocean exhibits the largest export of $CaCO_3$. The model calculates a total export of $CaCO_3$ of 0.190 Pg C yr^{-1} whcih is a low value compared to the global observations based estimate [Berelson et al., 2007].

Figure (18 b) exhibits the distribution of $CaCO_3$ (with CR = 0.02) export in the global ocean at 100 meter depth. This export distribution exhibits the same pattern as like as figure (18 a) but with a higher export value while export is maximum in the Indian Ocean. The total calculated amount of $CaCO_3$ export from the model is 0.379 Pg C yr^{-1}.

As these sensitivity analysis simulations contain same calcite equation but with different CR value, figure (18 c and d) (CR = 0.03 and 0.04 respectively) exhibit the same pattern but with higher export value due to higher calcification ratio. The model calculated total export value for $CaCO_3$ is 0.569 Pg C yr^{-1} (for CR = 0.03) and 0.758 Pg C yr^{-1} (for CR = 0.04).

The analysis of the alkalinity distribution of surface and depth, as well as the $CaCO_3$ export, shows that using a more complicated parameterization of the calcite equation does not improve the model results. The best model run (with CR = 0.01) leads to an average vertical profile of TA which is close to the observations, but there remain large positive and negative deviations from TA observed in the horizontal.

5 Summary and discussion

In this study, seven different model runs are performed over a period of 1000 years of integration time. Initially, a reference model run was perfomed without changing the existing standard setup to look upon the globally averaged vertical profile of alkalinity compared to the global observation (GLODAP). The observation from this reference run (fig. 19 a) compared to global observations is that alkalinity is shifted from the ocean surface to depth between 1000 m to 5000 m. Two different experimental model runs varying the calcification ratio (CR) have then been performed to validate the explanation that the model is in existing setup is doing much calcification and dissolution within the water column in the global ocean. Exp 01 and Exp 02 are performed with CR = 0.01 and 0.03 respectively and compared to the global observations (fig. 19 a). It is seen from (fig. 19 a) that Exp 01 (CR = 0.01) shows a much better profile than the reference run and Exp 02 compared to the global observations.

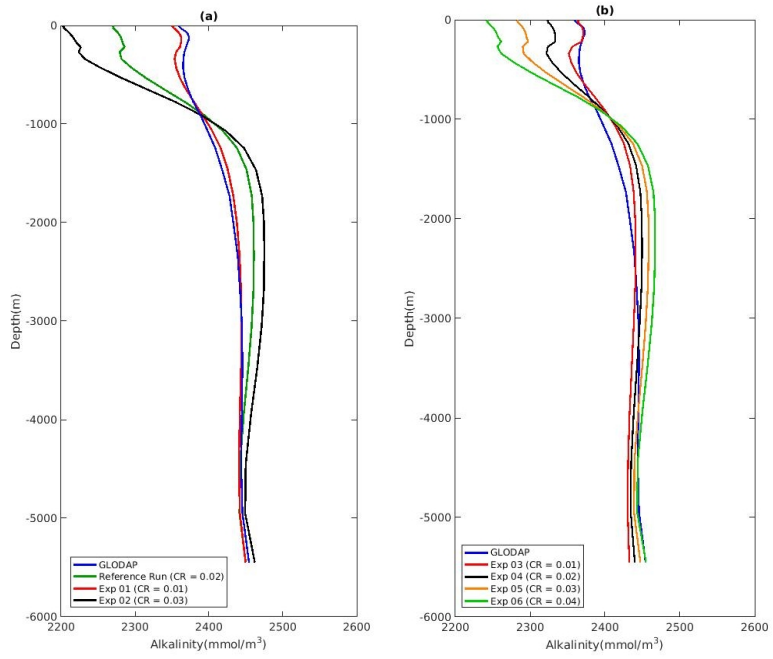

Figure 19: *Global average vertical profile of alkalinity varying CR compared to global observation (blue line); (a) shows alkalinity profile varying CR and (b) shows alkalinity profile with modified calcite equation, temperature dependency and different CR. Blue line represents the GLODAP data as global observation.*

Four new model simulations (Exp 03, Exp 04, Exp 05 and Exp 06) with a modified calcite equation which is carrying new parameterisations for the rain ratio exhibit differences in globally averaged vertical profile of alkalinity (fig. 19 b). Compared to the global observations, Exp 03 provides a better alkalinity profile among the four experiment with less shift of alkalinity from the Ocean surface to the mid layer depth. This shift of alkalinity is getting stronger with an increase in CR for Exp 04, Exp 05 and Exp 06.

Experiment name	RMS Value	Calcification Ratio (CR)	$CaCO_3$ export (Pg C yr^{-1})
Reference Run	60.566	0.02	0.685
Exp 01	7.316	0.01	0.343
Exp 02	102.298	0.03	1.028
Exp 03	9.534	0.01	0.190
Exp 04	27.829	0.02	0.379
Exp 05	52.596	0.03	0.569
Exp 06	77.770	0.04	0.758

Table 1: Numerical description of the seven different model run.

Exp 01 exhibits the minimal root mean square (RMS) value (table 1) for the difference between the globally averaged vertical alkalinity profile and the global observations. On the other hand Exp 03 shows a minimum RMS value (table 1) among the four experimental simulations with a modified calcite equation. Exp 04, 05 and 06 exhibits higher RMS value almost in an order of magnitude respectively compared to Exp 03.

As the three different model run (reference, Exp 01 and Exp 02) carries different CR value, Exp 01 with the lowest CR value of 0.01 shows the lowest value of $CaCO_3$ export among the three model run (table 1). Not surprisingly, a linear relationship is observed in between CR value and $CaCO_3$ export for these three model runs because changes in calcification in the model do not affect the productivity of the small phytoplankton.

In an analogous way, Exp 03 shows the lowest value of $CaCO_3$ export (table 1) among the four seperate model run (Exp 03, 04, 05 and 06) because of the lowest CR value set in the model. Here also a linear relationship is observed in between CR value and $CaCO_3$ export for these four different experimental model run. Exp 04, 05 and 06 exhibits higher $CaCO_3$ export value (0.379, 0.569 and 0.758 of Pg C yr^{-1} respectively) compared to Exp 01.

Furthermore, a basinwise anlysis is done to investigate the hydrological cycle effect on distribution of alkalinity in the global ocean by normalising alkalinity based on salinity. The alkalinity distributions (fig. 14) for the reference run and Exp 01 were compared to a global observation data set (fig. 13). The distribution of alkalinity (both Alk and Alk_1) for Exp 01 shows much better distribution than the reference run while comparing to the global observations.

From figure (19 a) and (19 b) it is undoubtedly clear that, Exp 01 and Exp 03 provide the best alkalinity profile among the seven different model runs. These two simulations have a reduced CR value (0.01) but a different calcite equation. As Exp 01 and Exp 03 have a lower production of $CaCO_3$ compared to the reference run (table 1), it is necessary to investigate how this reduction of $CaCO_3$ affects the carbon cycle. It is expected that a reduction in alkalinity at the surface will affect the carbon uptake by the ocean because at lower surface alkalinity for the same pCO_2, less carbon uptake will happen. An analysis of the global average DIC for the reference run, Exp 01 and Exp 03 from year 1000 (start of the model run) to year 2000 (end of the model run) is shown in figure (20).

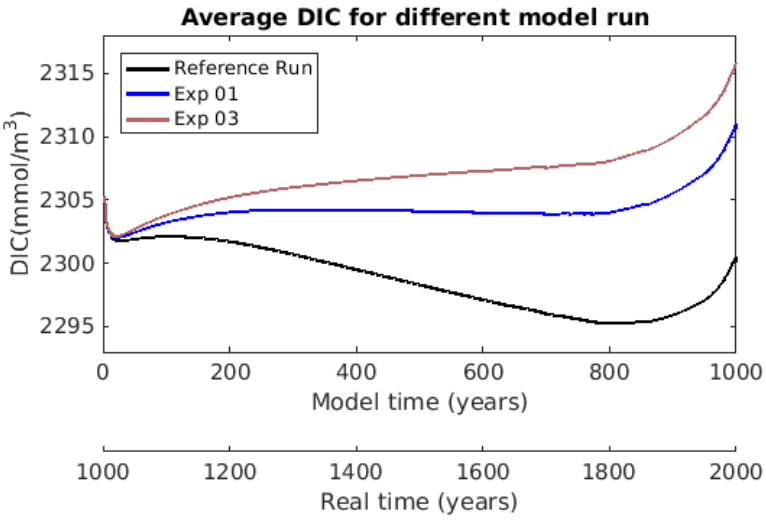

Figure 20: *Global average concentration of DIC for three different model runs with different calcification ratio (both in magnitude and pattern) over 1000 years of integration time.*

An rapid initial drop of DIC (i.e. some outgassing of CO_2 from the ocean into the atmosphere) by almost the same amount of 3 mmol m^{-3} which is 49.6 Pg of carbon (1 mmol m^{-3} = 16.53 Pg C) in the reference run, Exp 01 and Exp 03 is observed from figure (20). A possible explanation for this decrease is that the calculated pre-industrial DIC used in the model is only

a rough estimation; there is a bit too much DIC near the ocean surface for the given alkalinity and atmospheric pCO_2 of 280 ppm. In all three model runs also a rapid increase of DIC from year 1775 towards year 2000 (fig. 20) is observed which is caused by the increasing CO_2 in the atmosphere from fossil fuel burning and deforestation, leading to uptake of CO_2 in the ocean (the so-called 'anthropogenic carbon').

The three runs differ most in their long-term trend in DIC. In the reference run, DIC decreases (fig. 20) which is obvious as because of the decrease in surface alkalinity (as alkalinity is transported from the ocean surface to the mid layers depth (fig. 5) in the ocean). At lower surface TA, the ocean can hold less DIC for the same amount of CO_2 in the atmosphere. In Exp 01 and Exp 03 this does not happen; in Exp 01, the ocean seems to stay close to equilibrium because surface alkalinity stays almost constant (fig. 10 c). In Exp 03 there are some regions where surface alkalinity becomes to high at the end (fig. 10 c) and probably this leads to the observed slow increase in DIC as well.

To investigate furthermore, an analysis of annual average surface distribution of the sea to air CO_2 flux for the year 2000 is done for the reference run, Exp 01 and Exp 03 shown in figure (22). In this analysis, model results are compared with one of the best global observation of mean climatological mean annual sea-air flux for the year 2000 from [Takahashi et al., 2009], which is shown in figure (21).

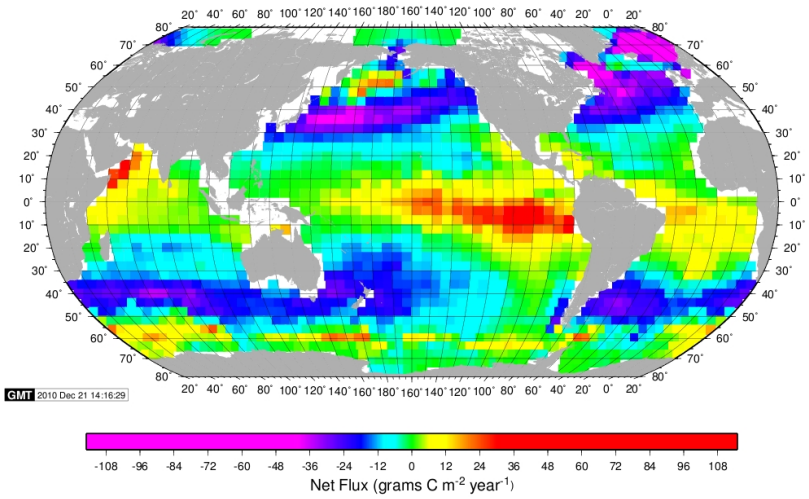

Figure 21: *Climatological mean annual sea-air CO_2 flux for the year 2000. [Takahashi et al., 2009]*

The patterns that are obtained from the different model runs (fig. 22), qualitatively are not so different compared to figure (21). The features of the patterns are following:

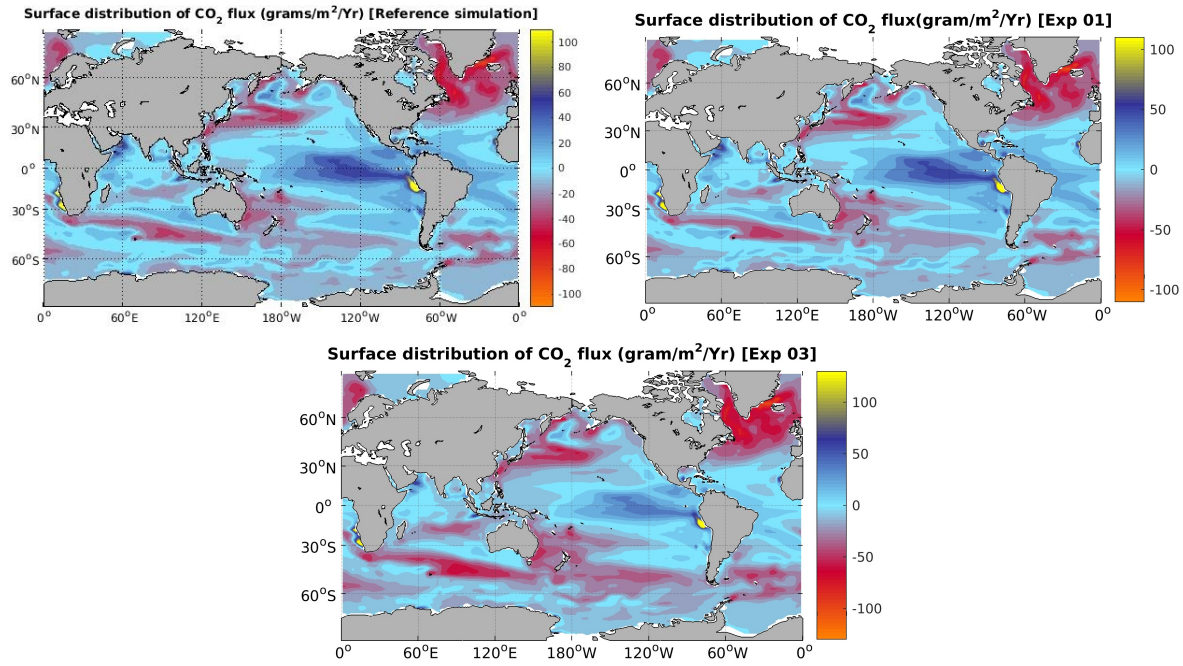

Figure 22: *Annual average surface distribution of CO_2 flux with different calcification ratio; top left image shows the distribution for the reference run, top right images shows EXP 01 and image at the bottom shows Exp 03.*

In the reference run, strong outgassing (ocean to atmosphere) is observed in the tropical Atlantic, North West Indian Ocean and in the Southern Ocean and the strongest outgassing is observed in the tropical Pacific Ocean. Strong uptake of CO_2 is observed in the North Atlantic, North-West Pacific and in the belt around the Antarctica. All theses features qualitatively agree with figure (21).

In the Exp 01 (fig. 22), a similar pattern is observed but with a stronger uptake of CO_2 and weaker outgassing compared to the reference run which also agree with figure (21).

In the Exp 03 (fig. 22), an almost identical pattern is observed compared to the reference run but with stronger uptake of CO_2 and less outgassing.

6 Conclusions

The production of $CaCO_3$ in the ocean and its dissolution within the water column are important processes that have a direct impact on dissolved inorganic carbon and alkalinity and hence CO_2 exchange between the ocean and the atmosphere. Production and dissolution of $CaCO_3$ is studied by using the global biogeochemical model (REcoM) which describes these processes in a relatively simplistic way. After integrating the model over a thousand year under a monthly climatological forcing, strong deviation in global alkalinity distribution in the ocean is identified with respect to the available observations when using the reference set of parameters of the model. In this case, the model transfers alkalinity from the ocean surface to the deep ocean, mostly in the depth range arround from 1700 to 2000 m. There are several possible explanations for that; changes in the distribution of freshwater or salinity, but more likely an unrealistic distribution of $CaCO_3$ production and dissolution in the model.

In this study it is tested whether an improvement in the modeled alkalinity distribution can be reached by changing the parameterization of the $CaCO_3$: POC production ratio in the model. It is shown that a simple reduction in the ratio leads to a much improved alkalinity distribution. A more complicated dependency of the $CaCO_3$: POC production rate on temperature, nutrients and biomass as suggested by [Aumont and Bopp, 2006] does not lead to a significant improvement.

The model run (Exp 01) that gives the best fit to the observed alkalinity distribution, however has a global export of $CaCO_3$ that is slightly lower than the estimation of [Berelson et al., 2007].

One aspect that is completely neglected in the current model, is the formation of $CaCO_3$ in the form of aragonite. It could be that the inclusion of aragonite, which dissolves more easily in the water column, leads to increased $CaCO_3$ export without changing alkalinity too much. Another aspect which has not been studied here is the dependency of the dissolution of $CaCO_3$ on seawater saturation state. The model so far neglects this dependency. To study the effect of this would be worthwile.

References

A. Adcroft, C. Hill, J.-M. Campin, J. Marshall, and P. Heimbach. Overview of the formulation and numerics of the MIT GCM. In *Proceedings of the ECMWF seminar series on Numerical Methods, Recent developments in numerical methods for atmosphere and ocean modelling*, pages 139–149, 2004.

A. L. Alldredge and Y. Cohen. Can Microscale Chemical Patches Persist in the Sea? Microelectrode Study of Marine Snow, Fecal Pellets. *Science*, 235(4789):689–691, 1987. doi: 10.1126/science.235.4789.689.

J. Antonov, D. Seidov, T. Boyer, R. Locarnini, A. Mishonov, H. Garcia, O. Baranova, M. Zweng, and D. Johnson. World Ocean Atlas 2009, Volume 2: Salinity, edited by: Levitus, S. *NOAA Atlas NESDIS*, 69, 2010.

D. Archer. Equatorial Pacific calcite preservation cycles: Production or dissolution? *Paleoceanography*, 6(5):561–571, 1991.

D. Archer, A. Winguth, D. Lea, and N. Mahowald. What caused the glacial/interglacial atmospheric pCO_2 cycles? *Reviews of Geophysics*, 38(2):159–189, 2000. doi: 10.1029/1999RG000066.

R. S. Arvidson, I. E. Ertan, J. E. Amonette, and A. Luttge. Variation in calcite dissolution rates: A fundamental problem? *Geochimica et Cosmochimica Acta*, 67(9):1623 – 1634, 2003. doi: 10.1016/S0016-7037(02)01177-8.

O. Aumont and L. Bopp. Globalizing results from ocean in situ iron fertilization studies. *Global Biogeochemical Cycles*, 20(2), 2006. doi: 10.1029/2005GB002591.

O. Aumont, J. C. Orr, P. Monfray, G. Madec, and E. Maier-Reimer. Nutrient trapping in the equatorial Pacific: The ocean circulation solution. *Global Biogeochemical Cycles*, 13(2): 351–369, 1999. doi: 10.1029/1998GB900012.

O. Aumont, E. Maier-Reimer, S. Blain, and P. Monfray. An ecosystem model of the global ocean including Fe, Si, P colimitations. *Global Biogeochemical Cycles*, 17(2), 2003.

G. Battaglia, M. Steinacher, and F. Joos. A probabilistic assessment of calcium carbonate export and dissolution in the modern ocean. *Biogeosciences*, 13(9):2823–2848, 2016. doi: 10.5194/bg-13-2823-2016.

W. M. Berelson, W. M. Balch, R. Najjar, R. A. Feely, C. Sabine, and K. Lee. Relating estimates of $CaCO_3$ production, export, and dissolution in the water column to measurements of $CaCO_3$ rain into sediment traps and dissolution on the sea floor: A revised global carbonate budget. *Global Biogeochemical Cycles*, 21(1):GB1024, 2007. doi: 10.1029/2006GB002803.

M. Boye, C. M. van den Berg, J. T. de Jong, H. Leach, P. Croot, and H. J. de Baar. Organic complexation of iron in the Southern Ocean. *Deep Sea Research Part I: Oceanographic Research Papers*, 48(6):1477–1497, 2001.

W. S. Broecker and T. Takahashi. *Thermodynamics in Geology*, chapter : The solubility of calcite in sea water, pages 365–379. Springer, 1977.

W.-J. Cai, X. Hu, W.-J. Huang, L.-Q. Jiang, Y. Wang, T.-H. Peng, and X. Zhang. Alkalinity distribution in the western North Atlantic Ocean margins. *Journal of Geophysical Research: Oceans*, 115(C8), 2010.

J.-M. Campin and H. Goosse. Parameterization of density-driven downsloping flow for a coarse-resolution ocean model in z-coordinate. *Tellus A*, 51(3):412–430, 1999.

H. J. de Baar, J. T. de Jong, R. F. Nolting, K. R. Timmermans, M. A. van Leeuwe, U. Bathmann, M. R. van der Loeff, and J. Sildam. Low dissolved Fe and the absence of diatom blooms in remote Pacific waters of the Southern Ocean. *Marine Chemistry*, 66(1):1–34, 1999.

S. Emerson and M. Bender. Carbon fluxes at the sediment-water interface of the deep-sea: calcium carbonate preservation. *Journal of Marine Research*, 39:139–162, 1981.

K. Friis, A. Körtzinger, and D. W. R. Wallace. The salinity normalization of marine inorganic carbon chemistry data. *Geophysical Research Letters*, 30(2), 2003. doi: 10.1029/2002GL015898. 1085.

C. H. Fry, T. Tyrrell, M. P. Hain, N. R. Bates, and E. P. Achterberg. Analysis of global surface ocean alkalinity to determine controlling processes. *Marine Chemistry*, 174:46–57, 2015. doi: http://dx.doi.org/10.1016/j.marchem.2015.05.003.

H. Garcia, R. Locarnini, T. Boyer, and J. Antonov. World Ocean Atlas 2009, vol. 4, Nutrients (Phosphate, Nitrate, Silicate), NOAA Atlas NESDIS, vol. 71. *US Gov. Print. Off., Washington, DC*, 2010.

J.-P. Gattuso and L. Hansson. *Ocean acidification*. Oxford University Press, 2011.

R. J. Geider, H. L. MacIntyre, and T. M. Kana. A dynamic regulatory model of phytoplanktonic acclimation to light, nutrients, and temperature. *Limnology and Oceanography*, 43(4):679–694, 1998.

P. R. Gent and J. C. McWilliams. Isopycnal mixing in ocean circulation models. *Journal of Physical Oceanography*, 20(1):150–155, 1990.

W. Gentleman, A. Leising, B. Frost, S. Strom, and J. Murray. Functional responses for zooplankton feeding on multiple resources: a review of assumptions and biological dynamics. *Deep Sea Research Part II: Topical Studies in Oceanography*, 50(22):2847–2875, 2003.

J. Hauck, C. Völker, T. Wang, M. Hoppema, M. Losch, and D. A. Wolf-Gladrow. Seasonally different carbon flux changes in the Southern Ocean in response to the southern annular mode. *Global Biogeochemical Cycles*, 27(4):1236–1245, 2013. doi: 10.1002/2013GB004600.

S. A. Henson, R. Sanders, and E. Madsen. Global patterns in efficiency of particulate organic carbon export and transfer to the deep ocean. *Global Biogeochemical Cycles*, 26(1):GB1028, 2012. doi: 10.1029/2011GB004099.

X. Jin, R. G. Najjar, F. Louanchi, and S. C. Doney. A modeling study of the seasonal oxygen budget of the global ocean. *Journal of Geophysical Research: Oceans*, 112(C5):C05017, 2007. doi: 10.1029/2006JC003731.

R. M. Key, A. Kozyr, C. L. Sabine, K. Lee, R. Wanninkhof, J. L. Bullister, R. A. Feely, F. J. Millero, C. Mordy, and T.-H. Peng. A global ocean carbon climatology: Results from Global Data Analysis Project (GLODAP). *Global Biogeochemical Cycles*, 18(4), 2004.

I. Kriest and A. Oschlies. On the treatment of particulate organic matter sinking in large-scale models of marine biogeochemical cycles. *Biogeosciences*, 5(1):55–72, 2008.

W. G. Large and S. G. Yeager. *Diurnal to decadal global forcing for ocean and sea-ice models: the data sets and flux climatologies*. NCAR technical notes. National Center for Atmospheric Research Boulder, 2004. doi: 10.5065/D6KK98Q6.

K. Lee, L. T. Tong, F. J. Millero, C. L. Sabine, A. G. Dickson, C. Goyet, G.-H. Park, R. Wanninkhof, R. A. Feely, and R. M. Key. Global relationships of total alkalinity with salinity and temperature in surface waters of the world's oceans. *Geophysical Research Letters*, 33(19), 2006. doi: 10.1029/2006GL027207. L19605.

R. Locarnini, A. Mishonov, J. Antonov, T. Boyer, H. Garcia, O. Baranova, M. Zweng, and D. Johnson. World Ocean Atlas 2009, vol. 1. *Temperature, NOAA Atlas NESDIS*, 68, 2010.

M. Losch, M. Schröder, S. Hohn, and C. Völker. High-Resolution Modelling of Phytoplankton Distribution and Adaptation. In G. Münster, D. Wolf, and M. Kremer, editors, *NIC Symposium 2008*, pages 289–296. John von Neumann-Institut für Computing, Jülich, 2008.

M. Losch, D. Menemenlis, J.-M. Campin, P. Heimbach, and C. Hill. On the formulation of sea-ice models. Part 1: Effects of different solver implementations and parameterizations. *Ocean Modelling*, 33(1):129–144, 2010.

J. Marshall, C. Hill, L. Perelman, and A. Adcroft. Hydrostatic, quasi-hydrostatic, and nonhydrostatic ocean modeling. *Journal of Geophysical Research: Oceans*, 102(C3):5733–5752, 1997.

F. J. Millero, K. Lee, and M. Roche. Distribution of alkalinity in the surface waters of the major oceans. *Marine Chemistry*, 60(1–2):111 – 130, 1998. doi: 10.1016/S0304-4203(97)00084-4.

E. Paasche. Coccolith formation. *Nature*, 193:1094–1095, 1962. doi: 10.1038/1931094b0.

H. Postma. The exchange of oxygen and carbon dioxide between the ocean and the atmosphere. *Netherlands Journal of Sea Research*, 2(2):258–283, 1964.

J. L. Sarmiento and N. Gruber. *Ocean Biogeochemical Dynamics*. Princeton University Press, 2006.

C. S. Sikes, R. D. Roer, and K. M. Wilbur. Photosynthesis and coccolith formation: inorganic carbon sources and net inorganic reaction of deposition. *Limnology and Oceanography*, 25 (2):248–261, 1980.

D. Stammer, C. Wunsch, R. Giering, C. Eckert, P. Heimbach, J. Marotzke, A. Adcroft, C. Hill, and J. Marshall. Volume, heat, and freshwater transports of the global ocean circulation 1993–2000, estimated from a general circulation model constrained by World Ocean Circulation Experiment (WOCE) data. *Journal of Geophysical Research: Oceans*, 108(C1), 2003.

T. Takahashi, S. C. Sutherland, R. Wanninkhof, C. Sweeney, R. A. Feely, D. W. Chipman, B. Hales, G. Friederich, F. Chavez, C. Sabine, et al. Climatological mean and decadal change in surface ocean pCO_2, and net sea–air CO_2 flux over the global oceans. *Deep Sea Research Part II: Topical Studies in Oceanography*, 56(8):554–577, 2009.

D. A. Wolf-Gladrow, R. E. Zeebe, C. Klaas, A. Körtzinger, and A. G. Dickson. Total alkalinity: The explicit conservative expression and its application to biogeochemical processes. *Marine Chemistry*, 106(1):287–300, 2007. doi: 10.1016/j.marchem.2007.01.006.

Y. Yamanaka and E. Tajika. The role of the vertical fluxes of particulate organic matter and calcite in the oceanic carbon cycle: Studies using an ocean biogeochemical general circulation model. *Global Biogeochemical Cycles*, 10(2):361–382, 1996.

R. E. Zeebe and D. A. Wolf-Gladrow. *CO_2 in seawater: Equilibrium, Kinetics, Isotopes*, volume 65 of *Elsevier oceanography series*. Elsevier, 2001.

I. Zondervan. *Influence of carbonate chemistry and other environmental factors on the chemical and isotopic composition of coccolithophores, with emphasis on calcification and photosynthetic carbon fixation*. PhD thesis, University of Bremen, 2001.

I. Zondervan. The effects of light, macronutrients, trace metals and CO_2 on the production of calcium carbonate and organic carbon in coccolithophores—a review. *Deep Sea Research Part II: Topical Studies in Oceanography*, 54(5):521–537, 2007.